LU TP 00–16
hep-ph/0005110
May 2000

Production and Hadronization of Heavy Quarks

E. Norrbin[1] and T. Sjöstrand[2]

Department of Theoretical Physics,
Lund University, Lund, Sweden

Abstract

Heavy long-lived quarks, i.e. charm and bottom, are frequently studied both as tests of QCD and as probes for other physics aspects within and beyond the standard model. The long life-time implies that charm and bottom hadrons are formed and observed. This hadronization process cannot be studied in isolation, but depends on the production environment. Within the framework of the string model, a major effect is the drag from the other end of the string that the c/b quark belongs to. In extreme cases, a small-mass string can collapse to a single hadron, thereby giving a non-universal flavour composition to the produced hadrons. We here develop and present a detailed model for the charm/bottom hadronization process, involving the various aspects of string fragmentation and collapse, and put it in the context of several heavy-flavour production sources. Applications are presented from fixed-target to LHC energies.

[1]emanuel@thep.lu.se
[2]torbjorn@thep.lu.se

1 Introduction

The light u, d and s quarks can be obtained from a number of sources: valence flavours in hadronic beam particles, perturbative subprocesses and nonperturbative hadronization. Therefore the information carried by identified light hadrons is highly ambiguous. The charm and bottom quarks have masses significantly above the $\Lambda_{\rm QCD}$ scale, and therefore their production should be perturbatively calculable. That is, they are not expected to be produced at any significant rate in nonperturbative processes [1], and they do not occur as valence flavours of the commonly used beam particles. A priori, they are therefore excellent probes of the underlying hard dynamics, whether that involves standard QCD processes or various kinds of new physics. They can also be identified in the data by techniques such as secondary vertices, prompt leptons or kinematical constraints (e.g. the small $m_{\rm D^*} - m_{\rm D} - m_\pi$).

In order to understand the character of the perturbative process that occurred, it is often necessary to know not only that a c/b quark was produced, but also its original energy and direction of motion. The assumption is then often made that the observed charm/bottom hadron accurately reflects the original quark. For instance, the quark momentum distribution may be scaled down by a convolution with the Peterson fragmentation function [2], while the direction is assumed unchanged. In other cases, like for the study of CP violation in the $\rm B^0$–$\overline{\rm B}^0$ system, the produced hadrons are at the focus of attention, and a simple ansatz is that the composition of B hadrons is independent of the production environment and symmetric between particles and antiparticles.

The assumption, that heavy quarks remain rather unaffected by the environment in which they are produced, has some support in the Heavy Quark Effective Theory (HQET) [3], although that framework is more concerned with questions of decay than of production. However, even if many of the effects we will consider here indeed die out roughly inversely to the mass of the heavy quark — the $\Lambda/m_{\rm Q}$ behaviour of HQET — evidence is that the numerator Λ of such a scaling relation often is large. Thus the large lifetime differences between the D mesons has an analogue in large production asymmetries between D mesons in hadronic collisions [4, 5, 6, 7, 8]. Even with a reduction by a factor 2–3 when moving from charm to bottom, large effects are therefore expected also in the latter case. Only top hadrons would have been reasonably immune, had the top quark been long-lived enough for top hadrons to form.

In order to study and understand the sizeable deviations from the simple picture, of perturbation theory results only minimally modified, it is necessary to have a realistic framework for nonperturbative effects. The Lund string fragmentation model [1] will be the starting point here. In this picture, the colour confinement field between a quark and an antiquark (or a diquark) is squeezed into a tube-like region, corresponding to a linear confinement potential. This couples the hadronization of a c/b quark to the flavour content and momentum of the other string end, i.e. provides an explicit dependence on the production environment. An extreme case is the string collapse, where the mass of a string only allows the production of one single hadron, which by necessity therefore combines the c/b quark with the flavour at the other string end, often one of the valence flavours of the incoming beams. Also less extreme situations can give noticeable effects, and only in the limit of large string masses can one expect to recover a simple description. However, this description can still be counterintuitive, in that the hadronization process can 'speed up' as well as 'slow down' the heavy hadron relative to the heavy quark. In terms of the easily observable consequences, like hadron flavour asymmetries, we therefore go from

huge effects at fixed-target experiments to tiny ones at the LHC, but in less obvious ways the effects remain large also at high energies. Furthermore, events at large energies tend to be composed of several strings, so even at the LHC a fraction of small-mass strings is produced.

The presence of such effects is implicit in the Lund model, and was studied qualitatively early on [9]. It is only the more recent higher-precision data sets [5, 6, 7, 8] that allow quantitative comparisons to be carried out, and thereby give the possibility to 'fine-tune' the model with respect to nonperturbative parameters. A study of this kind was presented in a recent letter [10], where we concentrated on the production of charm at fixed-target energies. In this longer description, we will expand the study in several directions: by considering more heavy-flavour production mechanisms, by including bottom as well as charm production, by covering a larger range of energies and by addressing a larger set of observables. In the process, further improvements have also been made in the model.

This paper is organized as follows. Section 2 contains the model description, from the perturbative production mechanisms to the various domains of the hadronization process. Sections 3 and 4 present some results. In section 3 the emphasis is on distributions that help explain how the basic aspects of the model work, with little regard whether distributions are observable or not. In section 4 the emphasis is shifted to observable results for charm or bottom production at some current or planned detectors, although explanations will sometimes rely on non-observable distributions. Finally, section 5 contains a summary and outlook.

2 Model description

Based on the concept of factorization, we here subdivide the process in two distinct phases, the perturbative one, where the heavy quarks are produced, and the nonperturbative one, where these quarks hadronize. Heavy-flavour cross sections thus are completely determined by the former phase, while observable event properties reflect a combination of the two.

2.1 Perturbative aspects

2.1.1 Production mechanisms

Several different production mechanisms can be envisaged for heavy flavours. Here we will concentrate on QCD processes in hadron–hadron collisions. The $\mathcal{O}(\alpha_s^2)$ leading-order (LO) graphs, $q\overline{q} \to Q\overline{Q}$ and $gg \to Q\overline{Q}$ [11], Fig. 1a-b, then form the starting point for the continued discussion.

One way to proceed is to add next-to-leading order (NLO) perturbative processes, i.e the $\mathcal{O}(\alpha_s^3)$ corrections to the above [12]. New graphs are $q\overline{q} \to Q\overline{Q}g$, $qg \to Q\overline{Q}q$ and $gg \to Q\overline{Q}g$. Additionally the leading-order processes are modified by virtual corrections. Depending on the choice of cut-off parameters, the latter may give negative differential cross sections in some regions of phase space. The divergences disappear in sufficiently inclusive distributions, so much phenomenological insight can be gained [13]. However, with our currently available set of calculational tools, the NLO approach is not so well suited for the exclusive Monte Carlo studies we have in mind here, where hadronization is to be added on to the partonic picture. Furthermore, also the NLO results, although exact to $\mathcal{O}(\alpha_s^3)$, would be modified in yet higher orders, e.g. by the resummed effects of

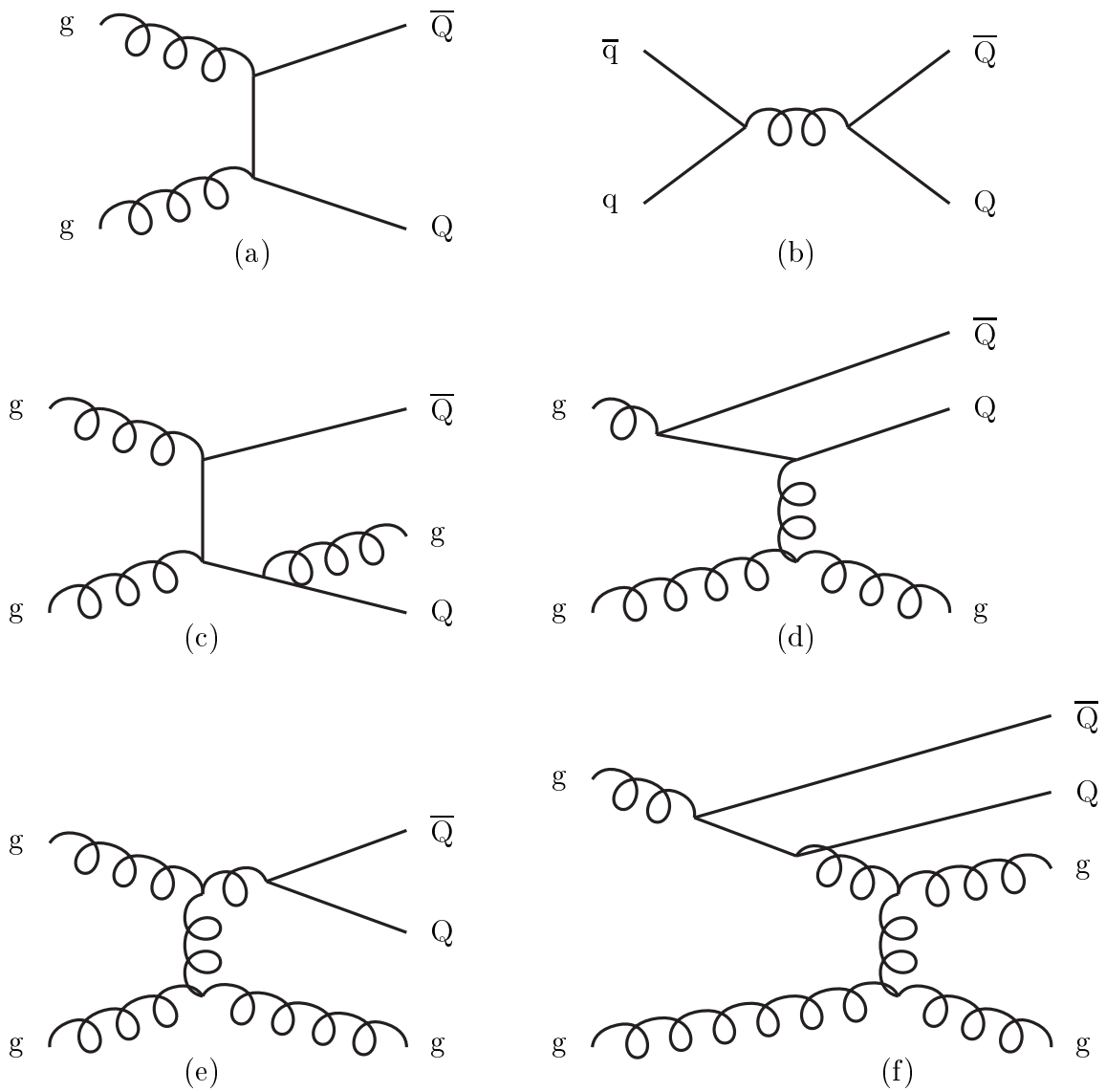

Figure 1: Examples of heavy-flavour production diagrams. (a,b) Leading order. (c) Pair creation (with gluon emission). (d) Flavour excitation. (e) Gluon splitting. (f) Events classified as gluon splitting but of flavour-excitation character.

multiple gluon emission [14].

As an alternative, the parton-shower (PS) approach offers a different set of approximations. It is not exact even to $\mathcal{O}(\alpha_{\mathrm{s}}^3)$, but it catches the leading-log aspects of the multiple-parton-emission phenomenon. Especially when one goes to higher energy this can offer many advantages. The PS approach is based on a probabilistic picture, wherein the overall $2 \to n$ partonic process is subdivided into three stages: initial-state cascades, hard scattering and final-state cascades. The hard scattering is here defined as the $2 \to 2$ sub-diagram that contains the largest virtuality, i.e. corresponds to the shortest-distance process. It is important to respect this in order to avoid double-counting, as will become apparent in the following. Heavy-flavour events can then be subdivided into three classes, which we will call pair creation, flavour excitation and gluon splitting. The names may be somewhat misleading, since all three classes create pairs at $\mathrm{g} \to \mathrm{Q}\overline{\mathrm{Q}}$ vertices, but it is in line with the colloquial nomenclature.

The three classes are characterized as follows.

1. Pair creation is when the hard subprocess is one of the two LO processes above. Showers do not modify production cross sections, but shift kinematics, Fig. 1c. For instance, in the LO description, the Q and $\overline{\mathrm{Q}}$ have to emerge back-to-back in azimuth in order to conserve momentum, while the parton shower allows a net recoil to be taken by one or several further partons.
2. Flavour excitation is when a heavy flavour from the parton distribution of one beam particle is put on mass shell by scattering against a parton of the other beam, i.e. $\mathrm{Qq} \to \mathrm{Qq}$ or $\mathrm{Qg} \to \mathrm{Qg}$, Fig. 1d. When the Q is not a valence flavour, it must come from a branching $\mathrm{g} \to \mathrm{Q}\overline{\mathrm{Q}}$ of the parton-distribution evolution. In most current-day parton-distribution parameterizations, heavy-flavour distributions are assumed to vanish for virtuality scales $Q^2 < m_{\mathrm{Q}}^2$. The hard scattering must therefore have a virtuality above m_{Q}^2. When the initial-state shower is reconstructed backwards [15], the $\mathrm{g} \to \mathrm{Q}\overline{\mathrm{Q}}$ branching will be encountered, provided that Q_0, the lower cutoff of the shower, obeys $Q_0^2 < m_{\mathrm{Q}}^2$. Effectively the processes therefore become at least $\mathrm{gq} \to \mathrm{Q}\overline{\mathrm{Q}}\mathrm{q}$ or $\mathrm{gg} \to \mathrm{Q}\overline{\mathrm{Q}}\mathrm{g}$, with the possibility of further emissions. In principle, such final states could also be obtained in the above pair-creation case, but the earlier advertised requirement on the hard scattering to be more virtual than the showers avoids double-counting.
3. Gluon splitting is when a $\mathrm{g} \to \mathrm{Q}\overline{\mathrm{Q}}$ branching occurs in the initial- or final-state shower, and no heavy flavours enter the hard scattering, Fig. 1e. Here the dominant source is gluons in the final-state showers, since timelike gluons emitted in the initial state are restricted to a smaller maximum virtuality. Except at high energy, most gluon splittings in the initial state instead result in flavour excitation, already covered above. An ambiguity of terminology exists with initial-state evolution chains where a gluon first branches to $\mathrm{Q}\overline{\mathrm{Q}}$ and the Q later emits another gluon that is the one to enter the hard scattering, Fig. 1f. From an ideological point of view, this is flavour excitation, since it is related to the evolution of the heavy-flavour parton distribution. From a practical point of view, however, we will choose to classify it as gluon splitting, since the hard scattering does not contain any heavy flavours.

In summary, the three classes above are then characterized by having 2, 1 or 0, respectively, heavy flavours in the final state of the hard subprocess. Of course, all this assumes that only one heavy-flavour pair is produced in an event — one could have e.g. double flavour excitation $\mathrm{QQ}' \to \mathrm{QQ}'$ — which normally is a good first approximation. Only in high-$p_\perp$ processes at high energies do profuse shower evolution make the multiple gluon-splitting process relevant.

To the above heavy-flavour sources, one could add the creation in decays of heavier resonances, such as $\mathrm{Z}^0 \to \mathrm{b}\overline{\mathrm{b}}$, $\mathrm{W}^+ \to \mathrm{c}\overline{\mathrm{s}}$, $\mathrm{H}^0 \to \mathrm{b}\overline{\mathrm{b}}$, $\mathrm{t} \to \mathrm{bW}^+$ and, of course, $\mathrm{b} \to \mathrm{c}$. In the current paper we will have little to say about these. However, c and b production at LEP 1 clearly provides the basis that we can build on here, by testing both the showering and the hadronization of heavy flavours, although in a different environment. For primary-produced heavy flavours, everything appears to be well understood in the framework of our models. Some discrepancies have been noted in the rate of hard gluon emission off b's [16], i.e. in the region where the shower is not expected to be perfect anyway, and even so discrepancies are tiny compared with typical uncertainties in hadronic collisions. Rather more worrisome is the observed rate of secondary heavy-flavour production, i.e. what we have called gluon splitting above. There the LEP observations exceed the rate predicted by shower programs [17, 18], and also by analytical calculations [19], by maybe as much as 50% [20, 19]. The error bars are large, however, so the true excess could be lower.

The possibility of higher rates already exists in some models [21], and one could imagine modifications to others. Currently the data is too poor to tell much about whether the shape agrees or not with models. We will therefore assume that only the rate could be a problem, and then any effect in hadronic collisions could be absorbed under the general heading of K factors, i.e. a rescaling in rate by higher-order corrections.

2.1.2 Parton-shower particulars

The perturbative shower approach is implemented in the PYTHIA program [17] that we will use for the studies in this paper.

Pair creation is easy to generate by itself, by allowing only the two hard processes $\mathrm{q\overline{q}} \to \mathrm{Q\overline{Q}}$ and $\mathrm{gg} \to \mathrm{Q\overline{Q}}$, using the LO matrix elements with quark masses included. The full phase space can be populated, i.e. down to $\hat{p}_\perp = 0$, since the quark mass provides the soft cutoff. The Q^2 scale of the process, used to set the range of allowed shower evolution as described below, is here taken to be $Q^2 = m_\mathrm{Q}^2 + \hat{p}_\perp^2$.

Flavour excitation can be obtained by only sampling the heavy flavour $\mathrm{Q}/\overline{\mathrm{Q}}$ from one of the incoming hadrons (a standard option of the program) while allowing all flavours from the other hadron. The two sides of the event are covered by two separate runs, added for the final results. We have not implemented any special matrix elements for the scattering of one heavy quark against another massless parton; instead massless matrix elements are used. Since the heavy-flavour parton distributions vanish for scales $Q^2 < m_\mathrm{Q}^2$, where we associate $Q^2 = \hat{p}_\perp^2 = \hat{t}\hat{u}/\hat{s}$ for massless kinematics, it follows that $\hat{s} > 4m_\mathrm{Q}^2$. The mass corrections to the matrix elements are therefore not expected to be very large. (In practice, massive four-vectors are constructed from the massless ones by a scaling-down of the three-momenta, in the rest frame of the subprocess, while preserving the energy: $p_i^2 = 0$, $p_i'^2 = m_i^2$, $\mathbf{p}_i' = \alpha \mathbf{p}_i$, $E_1' + E_2' = E_1 + E_2$. The actual $\hat{p}_\perp$ may thus end up somewhat below the nominal cut at m_Q.) The normal backwards shower evolution from the hard subprocess is then supposed to find a preceding $\mathrm{g} \to \mathrm{Q\overline{Q}}$ branching.

In the earlier PYTHIA versions, this often failed, and a heavy quark was allowed to form part of the beam-remnant flavour content that entered the nonperturbative description. We have now studied this phenomenon and recognized it as coming from the constrained kinematics that exists inside the shower. To see this point, consider a branching $\mathrm{g} \to \mathrm{Q\overline{Q}}$ where Q takes a fraction z of the lightcone momentum $p_+ = E + p_z$ of the gluon, and is virtual with $p_\mathrm{Q}^2 = -Q^2$. The recoiling $\overline{\mathrm{Q}}$ is part of the final state and must thus have mass m_Q, or above that if it radiates final-state gluons. Then conservation of $p_- = m_\perp^2/p_+$ gives

$$\frac{-Q^2 + p_\perp^2}{z} + \frac{m_\mathrm{Q}^2 + p_\perp^2}{1-z} = 0 \ , \tag{1}$$

and the requirement of a physical transverse momentum in the branching, $p_\perp^2 \geq 0$, translates into

$$z \leq \frac{Q^2}{m_\mathrm{Q}^2 + Q^2} \ . \tag{2}$$

It may then become kinematically impossible to find a gluon with $x_\mathrm{g} = x_\mathrm{Q}/z < 1$. Since many common parton distribution parameterizations do not respect the above kinematics constraints, we have introduced a further explicit check, where kinematically impossible configurations are rejected, and the cross section is reduced accordingly. Even when a Q is formally in the allowed region, one may feel threshold effects that make event generation less efficient. As a first approximation for this region, the shower is forced to 'try harder'

to find a $g \to Q\overline{Q}$ branching, without any loss of cross section. The end result is that, in the new program version, no c or b quarks remain in the beam remnant, but are always constructed as coming from a shower branching.

Gluon splitting cannot easily be generated by itself, since it could appear e.g. several steps down in a gluonic cascade, which cannot easily be predetermined. Instead it is necessary to attempt to generate the full QCD jet cross section, down to some lower $\hat{p}_{\perp\min}$ cut, and then pick up all events that 'happen' to contain the heavy flavour. Some events fall under the heading of pair creation or flavour excitation and are thus removed in a second step.

Note that the kinematics machinery here is based on massless quarks in the hard scattering, with some post-facto modifications for heavy quarks, so the alternative pair-creation description obtained here is less precise than the one in point 1 above. Masses are included in the description of the shower branching $g \to Q\overline{Q}$, however.

Showers should not populate kinematical regions already covered by the hard scattering. This requirement is not easy to implement exactly. One reason is that several different sets of constraints can appear, such as from virtuality ordering and angular ordering. Here we therefore satisfy ourselves with an approximate matching of $Q^2_{\max}$ and $M^2_{\max}$, the maximally allowed virtualities of spacelike and timelike showers, respectively, to $Q^2 = \hat{p}^2_\perp = \hat{t}\hat{u}/\hat{s}$, the conventional hard-scattering scale. This matching is generic to all branchings in showers, but obviously we give special attention to implications for the heavy-quark production vertices.

With massless kinematics, one may sensibly assume $Q^2 \leq Q^2_{\max}, M^2_{\max} \leq 4Q^2$. The lower limit would be appropriate for a t-channel graph, where $-\hat{t} \approx Q^2$ sets the maximal virtuality. The upper limit is more relevant for an s-channel graph, where $\hat{s} \geq 4\hat{p}^2_\perp$ sets the scale. So the above range translates into an uncertainty in the amount of shower evolution. However, we can try to be more specific. Timelike parton showers are evolved in terms of M^2, the squared mass of the propagating parton. It is thus akin to the $\hat{s}$ scale of the hard scattering, and $M^2_{\max} = 4Q^2$ is the preferred choice. With both Q and $\overline{Q}$ having a mass at or above m_Q, the heavy-flavour production threshold at $M^2_{\max} = 4m^2_Q$ then corresponds to $Q^2 = m^2_Q$, which agrees with the threshold for pair creation at the hard scattering. Spacelike parton showers instead are evolved in a spacelike virtuality, analogous to $\hat{t}$, and the reasonable choice then is $Q^2_{\max} = Q^2$. Again, this gives a matching threshold for 'flavour excitation' both in the shower and at the hard scattering, at m^2_Q for most heavy-flavour parton distribution parameterizations. Specifically, note that an initial-state shower branching does not have to produce two heavy quarks on mass shell, but only one at a time.

2.1.3 Parameters

The main formal parameters in the perturbative description are the heavy-quark masses. They enter in the description of hard scatterings and parton showers alike, both directly as mass terms in matrix elements or splitting kernels and indirectly in the description of the phase space. Therefore cross sections are especially sensitive to the value selected. Also the nonperturbative phenomenology is significantly affected. In [10], we chose to standardize on $m_c = 1.5$ GeV. Based on conventional mass formulae [22],

$$\frac{3m_{D^*} + m_D}{4} - m_c = \frac{3m_{B^*} + m_B}{4} - m_b \ , \tag{3}$$

we then obtain $m_b = 4.8$ GeV.

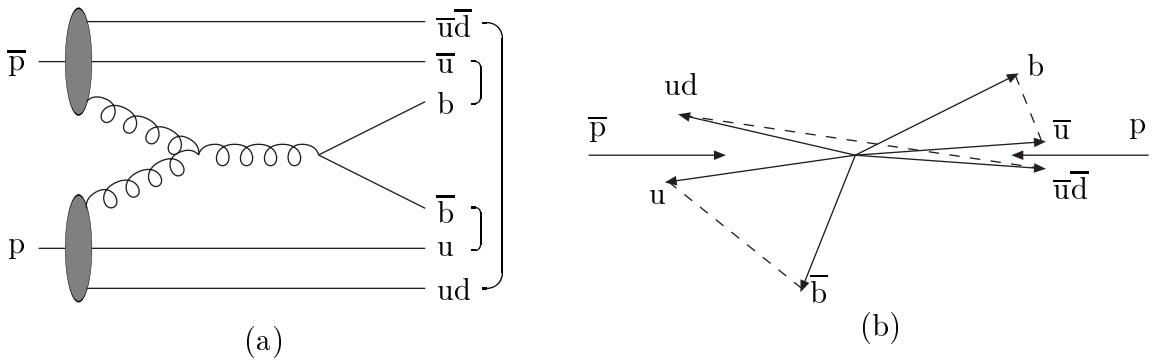

Figure 2: Example of a string configuration in a $p\overline{p}$ collision. (a) Graph of the process, with brackets denoting the final colour singlet subsystems. (b) Corresponding momentum space picture, with dashed lines denoting the strings.

Also the choice of parton distributions gives some leeway, especially since the gluon distribution is not yet so well constrained at small x and moderately small Q^2, where a non-negligible amount of the total charm/bottom cross section at high energies comes from. Unless otherwise specified, we have used the CTEQ 5L parameterized distributions for the proton [23], with $\Lambda^{(4)} = 0.192$ GeV. For the pion we rely on the GRV LO (updated) sets [24]. As already noted, the default factorization scale is $Q^2 = \hat{p}_\perp^2$.

2.2 Nonperturbative aspects

The way string fragmentation affects charm production was described in [10]. We will here develop the main points and outline the current status of our modeling, which is slightly modified since the previous publication.

The partonic state that is to be hadronized consists, at the very least, of the outgoing partons from the hard scattering and of the beam-remnant partons. Furthermore, a realistic study has to include the additional partons produced by initial- and final-state showers, and by the possibility of having several hard parton–parton interactions in the same event. These aspects increase in importance with increasing energy, and have to be included in the event description, but will not be at the focus of attention.

2.2.1 Colour flow

In the string model, confinement is implemented by spanning strings between the outgoing partons. These strings correspond to a Lorentz-invariant description of a linear confinement potential, with string tension $\kappa \approx 1$ GeV/fm. Each string piece has a colour charge at one end and its anticolour at the other. The double colour charge of the gluon corresponds to it being attached to two string pieces, while a quark is only attached to one. A diquark is considered as being in a colour antitriplet representation, and thus behaves (in this respect) like an antiquark. Then each string contains a colour triplet endpoint, a number (possibly zero) of intermediate gluons and a colour antitriplet end. An event will normally contain several separate strings.

The string topology can be derived from the colour flow of the hard process. For instance, consider the LO process $u\overline{u} \to b\overline{b}$ in a $p\overline{p}$ collision. The colour of the incoming u is inherited by the outgoing b, so the b will form a colour-singlet together with the proton remnant, here represented by a colour antitriplet ud diquark. In total, the event will thus contain two strings, one b–ud and one $\overline{b}$–$\overline{u}\overline{d}$. In $gg \to b\overline{b}$ a similar inspection

shows that two distinct colour topologies are possible. Representing the proton remnant by a u quark and a ud diquark (alternatively d plus uu), one possibility is to have three strings b–$\overline{\mathrm{u}}$, $\overline{\mathrm{b}}$–u and ud–$\overline{\mathrm{u}}\overline{\mathrm{d}}$, Fig. 2, and the other is the three strings b–ud, $\overline{\mathrm{b}}$–$\overline{\mathrm{u}}\overline{\mathrm{d}}$ and u–$\overline{\mathrm{u}}$.

In processes with several possible colour topologies, the relative composition may become nontrivial. For $\mathrm{gg} \to \mathrm{b}\overline{\mathrm{b}}$, the symmetry of the process gives an equal integrated — but not differential — rate for the two topologies. For a more illustrative example, consider e.g. ug $\to$ ug, again in $\mathrm{p}\overline{\mathrm{p}}$, which contains both s-, t- and u-channel graphs, including interference terms. There are again two possible colour topologies, u–$\overline{\mathrm{u}}$ plus ud–g–$\overline{\mathrm{u}}\overline{\mathrm{d}}$ and u–g–$\overline{\mathrm{u}}$ plus ud–$\overline{\mathrm{u}}\overline{\mathrm{d}}$. The u-channel only contributes to the former and the s-channel to the latter, but the t-channel contributes to both, meaning there is a nontrivial kinematics dependence on the relative probability for the two topologies. Furthermore, the cross section contains an interference contribution that corresponds to an undetermined colour flow, where it is not possible to subdivide the event into two separate colour singlets. Since the hadronic final state consists of singlets, clearly a collapse of this ambiguity must occur at some stage. We therefore subdivide the interference term, in a sensible but not unique way, between the two configurations above [25]. As should be expected, it is suppressed by a factor $1/N_C^2$, where $N_C = 3$ is the number of colours.

The above example carries over to flavour excitation $\mathrm{Qg} \to \mathrm{Qg}$, but additionally the colour flow in the initial- and final-state cascades has to be considered, at the very least the branching $\mathrm{g} \to \mathrm{Q}\overline{\mathrm{Q}}$. Since we only work to leading order, where no interference contributions are explicit (implicitly they have been used e.g. to introduce angular ordering in the shower evolution), this is straightforward: a new colour-anticolour pair is created and spanned between the daughters in $\mathrm{g} \to \mathrm{gg}$ and $\mathrm{q} \to \mathrm{qg}$, while the existing colours are split in $\mathrm{g} \to \mathrm{q}\overline{\mathrm{q}}$. No special colour rules are needed for heavy flavours. The last vertex, although the most rare of the three, has a special rôle in subdividing one colour singlet into two. With increasing energy and parton-shower activity, it gives an increasing average number of separate singlets in an event.

2.2.2 Hadronization

Once the string topology has been determined, the Lund string fragmentation model [1] can be applied to describe the nonperturbative hadronization. To first approximation, we assume that the hadronization of each colour singlet subsystem, i.e. string, can be considered separately from that of all the other subsystems. Presupposing that the fragmentation mechanism is universal, i.e. process-independent, the good description of $\mathrm{e}^+\mathrm{e}^-$ annihilation data should carry over. The main difference between $\mathrm{e}^+\mathrm{e}^-$ and hadron–hadron events is that the latter contain beam remnants which are colour-connected with the hard-scattering partons. More about these remnants below, in Sect. 2.2.3.

Depending on the invariant mass of a string, practical considerations lead to the need to distinguish three hadronization prescriptions:

1. *Normal string fragmentation.* In the ideal situation, each string has a large invariant mass. Then the standard iterative fragmentation scheme, for which the assumption of a continuum of phase-space states is essential, works well. The average multiplicity increases linearly with the string 'length', which means logarithmically with the string mass. In practice, this approach can be used for all strings above some cut-off mass of a few GeV.
2. *Cluster decay.* If a string is produced with a small invariant mass, maybe only two-body final states are kinematically accessible. The continuum assumption above

then is not valid, and the traditional iterative Lund scheme is not applicable. We call such a low-mass string a cluster, and consider it separately from above. When kinematically possible, a Q–$\overline{\mathrm{q}}$ cluster will decay into one heavy and one light hadron by the production of a light quark–antiquark pair in the colour force field between the two cluster endpoints, with the new quark flavour selected according to the same rules as in normal string fragmentation. The $\overline{\mathrm{q}}$ cluster end or the new $\mathrm{q}\overline{\mathrm{q}}$ pair may also denote diquarks; for ease of notation we will not always enumerate all the possible combinations covered in the full description.

3. *Cluster collapse.* This is the extreme case of the above situation, where the string mass is so small that the cluster cannot decay into two hadrons. It is then assumed to collapse directly into a single hadron, which inherits the flavour content of the string endpoints. The original continuum of string/cluster masses is replaced by a discrete set of hadron masses, mainly D/B and $\mathrm{D}^*/\mathrm{B}^*$ (or corresponding baryon states). This mechanism plays a special rôle, in that it allows large flavour asymmetries in favour of hadron species that can inherit some of the beam-remnant flavour content.

We assume that the nonperturbative hadronization process does not change the perturbatively calculated total rate of charm production. By local duality arguments [26], we further presume that the rate of cluster collapse can be obtained from the calculated rate of low-mass strings. This is related to the argument used in the $\mathrm{e}^+\mathrm{e}^- \to \mathrm{c}\overline{\mathrm{c}}$ channel, that the cross section in the J/ψ and ψ' peaks is approximately equal to a purely perturbatively calculated $\mathrm{c}\overline{\mathrm{c}}$ production cross section restricted to the below-$\mathrm{D}\overline{\mathrm{D}}$-threshold region. Similar relations have also been studied e.g. for τ decay to hadrons [27], and there shown to be valid to good accuracy. In the current case, the presence of other strings in the event additionally allows soft-gluon exchanges to modify parton momenta as required to obtain correct hadron masses. Traditional factorization of short- and long-distance physics would then also protect the charm cross section. Local duality and factorization, however, do not specify *how* to conserve the overall energy and momentum of an event, when a continuum of $\overline{\mathrm{c}}\mathrm{d}$ masses is to be replaced by a discrete D^- one. This will therefore be one of the key points to be studied below.

A first step towards constructing a model is to decide which mass range a string belongs to. We have above settled for $m_{\mathrm{c}} = 1.5$ GeV and $m_{\mathrm{b}} = 4.8$ GeV. Light quarks are given constituent masses, $m_{\mathrm{d}} = m_{\mathrm{u}} = 0.33$ GeV and $m_{\mathrm{s}} = 0.5$ GeV. Diquark masses are essentially the sum of the constituent masses above, with a spin-splitting term added. If the string invariant mass exceed the sum of the two string endpoint masses by some margin, $\sim$1 GeV, the normal string fragmentation routine can be used. This routine can produce two, three or more hadrons from the string, with the actual multiplicity determined dynamically during the hadronization process. Close to the lower limit, the two-body states dominate, so there should be a smooth transition to the cluster decay description.

For smaller string masses, a special cluster fragmentation procedure is used. Whether this results in the production of one or two hadrons depends on the assumed two-body threshold behaviour. Consider a $\mathrm{c}\overline{\mathrm{u}}$ cluster, for instance. In one extreme point of view, a $\mathrm{D}\pi$ pair should always be formed when above this threshold, and a single D never. In another extreme, the two-body fraction would gradually increase at a succession of thresholds: $\mathrm{D}\pi$, $\mathrm{D}^*\pi$, $\mathrm{D}\rho$, $\mathrm{D}^*\rho$, etc., where the relative probability for each channel is given by the standard flavour and spin mixture in string fragmentation. (For instance, D^* and D are assumed to be produced in the 3:1 ratio implied by spin counting, while the big ρ–π mass splitting there gives a mixture more like 1:1.) In our current default model, we

have chosen to steer a middle course, by allowing two attempts to find a possible pair of hadrons. Thus a fraction of events may collapse to a single resonance also above the Dπ threshold, but Dπ is effectively weighted up. For instance, a 2.2 GeV string mass might, in a first round, be chosen to decay to D$^*\rho$, and thus fail. If a second attempt instead gives Dπ, this two-body state would be accepted, but if D$^*\rho$ is selected again, the cluster would collapse to a single hadron. If a large number of attempts had been allowed (this can be varied as a free parameter), collapse would only become possible for cluster masses below the Dπ threshold.

One might have chosen also to include a phase-space factor close to each two-body threshold, instead of the step function used here. However, measurements of R in $\mathrm{e^+e^-}$ above the charm and bottom thresholds [28] indicate that Coulomb final-state interaction effects cancel any such suppression. (Actually, the same data could be used to argue for having only two-body states above the Dπ threshold. However, there is a difference: in a hadronic environment there will be a competition between the production of one or of two hadrons, while collapse to a single particle is not an option in $\mathrm{e^+e^-}$ away from the $\mathrm{c\overline{c}}$ resonance masses. Within the large error bars of the data, one might also read in some trend towards a larger R a bit further above the $\mathrm{D\overline{D}}$ threshold.)

In a cluster decay to two particles, a simplified version of normal string fragmentation is used, in a spirit similar to the machinery for joining the fragmentation chain by the production of two final hadrons somewhere in the middle of a normal string. In the cluster rest frame, a string direction is defined by the momentum vector of the heavy quark Q. As a starting distribution, the cluster is allowed to decay isotropically to the two hadrons. The hadronic transverse momentum with respect to this direction is then used to introduce a Gaussian suppression factor $\exp(-p_\perp^2/2\sigma^2)$, with $\sigma = 0.36$ GeV denoting the standard fragmentation $p_\perp$ width parameter. At threshold the decay thereby remains isotropic, but at (an imagined) large cluster mass one would reproduce the same $p_\perp$ spectrum as when a string breaks by the production of a new $\mathrm{q\overline{q}}$ pair. The heavy hadron H could still equally likely be produced in the Q hemisphere as in the opposite one, however. In string fragmentation, these two configurations enter with different relative weights, that can be derived from the space-time history of the process. Applied to the current case, this gives

$$\mathcal{P}_{\mathrm{opposite}} = \frac{1}{1+e^{b\Delta}} \qquad \text{with} \qquad \Delta = \sqrt{(m^2 - m_{\perp\mathrm{H}}^2 - m_{\perp\mathrm{h}}^2)^2 - 4m_{\perp\mathrm{H}}^2 m_{\perp\mathrm{h}}^2}\,, \tag{4}$$

where m is the cluster mass, $m_{\perp\mathrm{H}}$ and $m_{\perp\mathrm{h}}$ are the heavy and light hadron transverse masses, and b the string fragmentation parameter, $b \approx 0.9$ GeV^{-2}. $\Delta = \Gamma_2 - \Gamma_1 = \kappa^2(\tau_2^2 - \tau_1^2)$ is the difference in string area Γ_i spanned for the two solutions, which can be related to a difference in decay proper times τ_i by the string tension κ. After this final correction, giving the 'natural' ordering with the heavy hadron usually close to the direction of the heavy quark when well above the threshold, the transition between normal string fragmentation and cluster decay is reasonably smooth.

What is not so smooth is the cluster collapse mechanism. Here confinement effects have to project the continuum of string masses onto the observed discrete hadron mass spectrum. Because of the aforementioned local duality and factorization arguments, the total area of the spectrum should be conserved in the process. How the projection should be done is not known from first principles, however.

One conceivable strategy could be to introduce a weight function consisting of δ function peaks at the single-hadron masses, with suitably adjusted normalizations, and then step functions at the two-particle thresholds. This weight function, when multiplied with the partonic mass spectrum, should then give the hadron-level mass spectrum. Such an

approach is not well suited for Monte Carlo simulation, since the string mass is a complicated function of a number of variables and therefore the δ function cannot easily be integrated out. Conceptually, it would also suffer from the problem of having to have a non-universal weight function: the coefficients would have to be adjusted somewhat as a function of energy to ensure exact conservation of the total cross section, since the cluster mass spectrum itself is somewhat energy dependent. However, on general grounds, we do not expect the overall distribution of event characteristics to differ significantly between events with a $\overline{\mathrm{c}}$–d string mass exactly equal to the D^- one, and events where the string mass is maybe 100 MeV off. An appealing shortcut therefore is to accept all partonic configurations and thereafter introduce some 'minimal' adjustments to the kinematics to allow hadrons to be produced on the mass shell. Such a strategy would be consistent not only with local duality arguments, but also with the presence of soft final-state interactions, i.e. the exchange of nonperturbative gluons that can carry some amount of momentum between the low-mass string and the surrounding hadronic system. In the following we will therefore adopt the language of 'gluons' transferring energy and momentum between the strings in a collision, while leaving unanswered the question on the exact nature of those 'gluons'. Specifically, we will not address the possibility of changes in the colour structure of events by such 'gluons'.

The basic strategy will be to exchange some minimal amount of momentum between the collapsing cluster and other string pieces in its neighbourhood. Consider an event in its CM frame, with all partons emerging from an assumed common origin. Partons move out with close to the speed of light, so if they move in the same direction they also stay close to each other for a long time, and therefore have an enhanced chance to exchange momenta. An exchange can also occur to the string pieces spanned between the partons, quarks or gluons. The piece between two partons 1 and 2 spans the set of velocity vectors

$$\mathbf{v}_{\mathrm{string}} = \alpha \mathbf{v}_1 + (1-\alpha)\mathbf{v}_2 \ , \ 0 \leq \alpha \leq 1 \ . \tag{5}$$

A closest 'distance' between this string piece and the cluster can then be defined as

$$D^2 = \min_{0 \leq \alpha \leq 1} (\mathbf{v}_{\mathrm{cl}} - \mathbf{v}_{\mathrm{string}})^2 \ . \tag{6}$$

Based on this measure, the string piece closest to the cluster is found.

The momentum transfer can be in either direction, depending on whether the hadron is heavier or lighter than the cluster it comes from, $m_{\mathrm{H}} \gtrless m_{\mathrm{cl}}$. The hadron species, and thereby hadron mass, is selected according to the standard flavour selection rules. That is, there is no mass dependence, e.g. so that a lighter cluster could have been more likely to form a D/B and a heavier a $\mathrm{D}^*/\mathrm{B}^*$; after all, the mass splitting is not so large that kinematics should come out particularly different for the two.

The simpler situation is when $m_{\mathrm{H}} < m_{\mathrm{cl}}$. Then one may split the cluster four-momentum into two parallel vectors, $p_{\mathrm{H}} = (m_{\mathrm{H}}/m_{\mathrm{cl}})p_{\mathrm{cl}}$ and $p_{\mathrm{g}} = (1 - m_{\mathrm{H}}/m_{\mathrm{cl}})p_{\mathrm{cl}}$. The latter momentum, for an imagined gluon, can be absorbed by the closest string piece found above, i.e. be inserted between the endpoint partons 1 and 2. This gluon has $m_{\mathrm{g}}^2 > 0$, but not too large or a collapse would not have occurred. Such somewhat massive gluons are well modeled by the standard string fragmentation framework [29]. One could have chosen a 'decay' of the cluster into a massless gluon, e.g. with an isotropic angular distribution in its rest frame, but such an ansatz gives the same average behaviour as the one above, and only slight differences in fluctuations.

A worse situation is when $m_{\mathrm{H}} > m_{\mathrm{cl}}$. A negative-energy gluon could be defined and handled as above. Usually this works fine, but it can lead to complete strings (not just

string pieces) with negative m^2, or even to hadrons with $|x_{\rm F}| > 1$, so such an approach is not quite trustworthy. Instead we assume an exchange in the opposite direction, where the nearest string piece emits a gluon that can be absorbed by the cluster to give it the desired hadron mass. To be more precise, form a weighted sum of the endpoint momenta

$$p_s = \alpha p_1 + \beta p_2 = \frac{p_2 p_{\rm cl}}{p_1 p_2} p_1 + \frac{p_1 p_{\rm cl}}{p_1 p_2} p_2 \ , \tag{7}$$

so that the end of the string that is closest to the cluster is weighted up relative to the one further away. Thereafter define

$$p_{\rm H} = p_{\rm cl} + \delta p_s \ , \tag{8}$$

with δ determined by the constraint $p_{\rm H}^2 = m_{\rm H}^2$. The hadron will then have the correct mass, and the string endpoint momenta are scaled down by factors $1 - \delta\alpha$ and $1 - \delta\beta$, respectively. (Also the endpoint masses are scaled down in the process. This is no problem, since the string fragmentation is not dependent on having partons of a fixed mass.)

In the rare case that, e.g., $1 - \delta\alpha < 0$, the procedure has to be extended. If the parton 1 is a gluon, the string does not end there but extends further to a parton 3. Then the gluon 1 four-momentum can be fully absorbed by the cluster, and the procedure above repeated for the partons 2 and 3. That way, one gluon after the next could be absorbed, at least in principle. If instead a string endpoint is involved, this trick does not work and we there revert to the old scheme, where four-momentum is shuffled between the cluster and the parton furthest away from it, i.e. with the largest cluster+parton invariant mass. This scheme is more robust, and normally requires only small four-momentum transfers, but physically it is not so appealing, since it runs counter to the principle of locality in the hadronization description. In practice, though, there is a good general agreement between results for the new and the older description [10].

2.2.3 Beam remnants

A characteristic feature of hadronic collisions is the presence of a beam remnant. This remnant is defined by what is left behind of the hadron by the initial-state parton shower initiator. In the simplest case, when a valence quark is picked out of the incoming hadron, the remnant is a single antiquark, for a meson, or a diquark, for a baryon. In either case it is in a colour antitriplet state that can be considered as a unit. For a baryon, simple flavour+spin SU(6) rules can be used, e.g. to select between a $\rm ud_0$ and a $\rm ud_1$ diquark.

A more complex situation is when a gluon is picked out of the hadron, so that the remnant is a colour octet, i.e. attached to two strings. A convenient approach is to imagine this system split into two separate string endpoints, one colour triplet and the other antitriplet. For a meson this would correspond to valence quark+antiquark, for a baryon to quark+diquark. The beam remnant distribution function (BRDF) is introduced to describe how the (light-cone) momentum of the remnant is shared between the two, in fractions χ and $1 - \chi$, respectively. For an octet meson remnant the χ distribution is always implicitly symmetrized between the q and $\overline{\rm q}$, while for an octet baryon remnant one quark (picked at random among the three) takes the fraction χ and the remaining colour antitriplet diquark $1 - \chi$. There is no first-principles theory for BRDF's, so one has to rely on sensible ansätze. It turns out that asymmetries, e.g. between D and $\overline{\rm D}$ mesons, are very sensitive to the choices made here, especially in the baryon fragmentation regions [10]. Therefore we will have reason to compare different forms. As an intermediate, default,

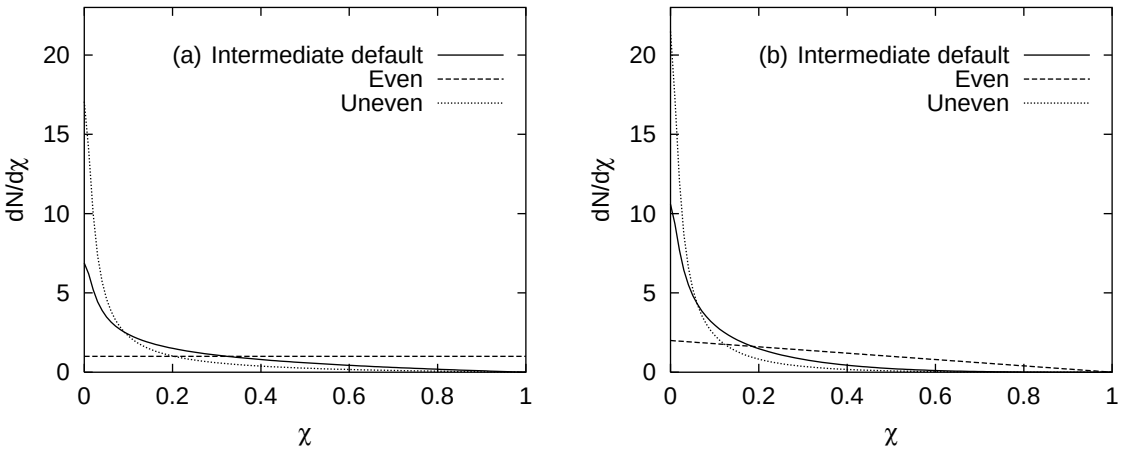

Figure 3: Distribution of χ variable at 40 GeV for (a) a meson and (b) a baryon. Full curves show the default intermediate option, dashed the even one and dotted the uneven one, corresponding to $\langle\chi\rangle = 0.22$, 0.50 and .12 for mesons and .13, .33 and .076 for baryons.

option we use

$$\begin{aligned} f(\chi) &\propto \frac{1-\chi}{\sqrt[4]{\chi^2 + c_{\min}^2}} \qquad \text{for mesons,} \\ f(\chi) &\propto \frac{(1-\chi)^3}{\sqrt[4]{\chi^2 + c_{\min}^2}} \qquad \text{for baryons,} \end{aligned} \tag{9}$$

see Fig. 3. Here $c_{\min} = 0.6$ GeV$/E_{\mathrm{CM}} \approx 2m_{\mathrm{q}}/E_{\mathrm{CM}}$ provides an effective damping for χ values so small that a parton ends up in the opposite hemisphere from its mother hadron. Some arguments for the forms above, especially the $1/\sqrt{\chi}$ behaviour, can be found in reggeon phenomenology [30], but basically this is just a compromise between extremes. One such is that of an even sharing between all the valence partons,

$$\begin{aligned} f(\chi) &= 1 \qquad \text{for mesons,} \\ f(\chi) &= 2(1-\chi) \qquad \text{for baryons.} \end{aligned} \tag{10}$$

Another is that of an uneven distribution,

$$\begin{aligned} f(\chi) &\propto \frac{1-\chi}{\sqrt{\chi^2 + c_{\min}^2}} \qquad \text{for mesons,} \\ f(\chi) &\propto \frac{(1-\chi)^3}{\sqrt{\chi^2 + c_{\min}^2}} \qquad \text{for baryons,} \end{aligned} \tag{11}$$

reminiscent of the parton distributions encountered in the process of perturbatively extracting a parton from a hadron.

Also sea quarks/antiquarks may be emitted from a hadron. We here refer to the lighter u, d and s quarks that, unlike the heavier quarks, exist in the parton distributions at the lower shower cut-off scale $Q_0 \approx 1$ GeV. In this case, the remnant is in an (anti)triplet state, which conveniently is subdivided into a colourless hadron plus a simple coloured remnant. For instance, a uuds remnant could become $\Lambda + \mathrm{u}$. The current default is to assign the hadron a χ lightcone fraction according to the normal string fragmentation

function. Differences relative to using simpler expressions, in the spirit e.g. of the even sharing above, are minor for the quantities of interest to us. One reason is that the sea contribution is much smaller than the gluon one above. A questionable but convenient approximation is to assume that any emitted quark that could be a valence quark also is one; a better choice would be to split e.g. the u distribution of the proton into one valence and one sea part that are to be handled differently. This simplification is not so critical, for the same reason as above.

The partons entering the hard interaction are traditionally taken to have a non-vanishing primordial $k_\perp$. In a shower description, such a $k_\perp$ is instead assigned to the initial-state shower initiators. These could be seen as having a purely nonperturbative Fermi motion inside the incoming hadrons. Typical values should thus be 300–400 MeV, consistent with constituent quark masses and fragmentation transverse momenta (σ above). The initial-state shower will add further activity, so the parton that enters the hard $2 \to 2$ subprocess could well have more. However, in many connections [31], also for charm production at fixed-target energies [13], it has been noted that much higher values are required, at or even above 1 GeV. This remains somewhat of a mystery, which we do not attempt to solve here. We will use a Gaussian width of 1 GeV as default. The choice of primordial-$k_\perp$ distribution is of non-negligible importance, both by providing a $p_\perp$ kick to the produced heavy-flavour quarks and, by momentum conservation, an opposite kick to the beam remnants.

When a remnant is split up in two, not only longitudinal but also transverse momentum sharing has to be specified. If the large primordial $k_\perp$ comes from a complicated multigluon emission process, there is no reason why all of it should be taken by one of the remnants. Instead it is assumed shared evenly between the two. Furthermore, a relative kick is added between them, picked according to the standard fragmentation $p_\perp$ width σ, for simplicity and in the lack of any experimental indication.

A further aspect of the beam-remnant physics is the possibility of having multiple parton–parton interactions in an event. This could have an impact in a number of ways. Some of these, like an increase of the underlying event activity and more complicated string drawings, are included in the standard Pythia framework [32], but obviously with several degrees of freedom in the description. Others, like the production of multiple heavy-flavour pairs in separate hard processes and the possibility of even more complicated beam remnants than the ones above, have not (yet) been studied.

Another area not addressed is that of QCD interconnection, wherein a given colour configuration may be rearranged by soft-gluon exchanges [33]. Mechanisms in this spirit have been proposed e.g. to produce closed-heavy-flavour states (J/ψ etc.) from colour-octet heavy-flavour pairs [34].

These examples serve as useful reminders that the modelling, however sophisticated, cannot be considered as complete in the nonperturbative sector. Therefore one cannot hope for perfect agreement between the model and the data. In the following we will show, however, that the current experimental data can be understood qualitatively, and often also quantitatively. This gives some confidence that the modeling described above is a good first approximation, that could also be used for predictions in processes or at energies not yet studied.

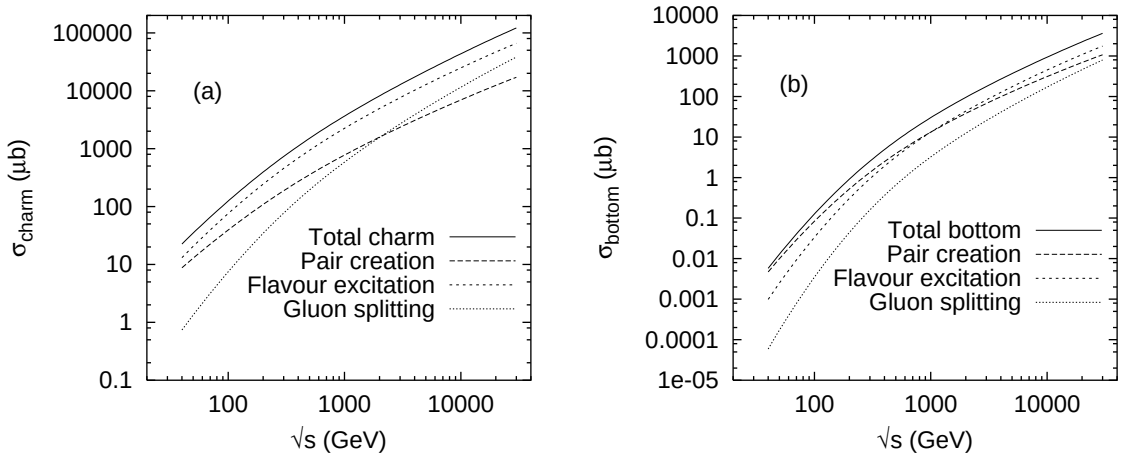

Figure 4: The total (a) charm and (b) bottom cross sections for pp collisions as a function of $E_{\mathrm{CM}} = \sqrt{s}$. The contributions from pair creation, flavour excitation and gluon splitting are shown separately.

3 Simple model properties

In this section we examine some properties of the model as presented in the previous section. In the first part we study purely perturbative properties of the model such as the total cross section, $\hat{p}_\perp$ of the hard interaction and quark distributions. In the second part we study the properties of the nonperturbative fragmentation. Experimental observables will be presented and confronted with data in the next section.

3.1 Properties of the perturbative production

Above, three different production channels have been distinguished in the parton-shower description: pair creation, flavour excitation and gluon splitting. In the following we will present their separate contributions, even though this subdivision of course is unobservable and model-dependent. It will still provide helpful insights.

The most basic and inclusive observable is the total heavy-flavour cross section. In Fig. 4 we present it as a function of the pp center-of-mass energy, from the fixed-target régime to LHC and beyond, both for charm and bottom. The cross section is divided into the contributions from the three perturbative production channels. As noted before, we assume that no nonperturbative effects contribute to the total cross section. The level of the total cross section is in sensible agreement with the present data (not shown), indicating that there is no need for any further significant production mechanism.

For small (fixed-target) energies the pair creation cross section is dominating the production, followed by a non-negligible fraction of flavour excitation, whereas gluon splitting is very small. As the energy is increased, flavour excitation overtakes pair production and gluon splitting is catching up. At very large energies gluon splitting becomes the dominant production mechanism, so that the low-energy pattern is completely reversed.

The reason is not so difficult to understand. If we think of any partonic process, it will only contain one hardest $2 \to 2$ scattering whatever the energy, whereas the number of branchings in the associated initial- and final-state showers will increase with energy. This increase comes in part from the the growing phase space, e.g. the larger rapidity evolution range of the initial-state cascades, in part from the increase in accessible and typical virtuality scales Q^2 for the hard subprocess. The multiplication effect is at its full

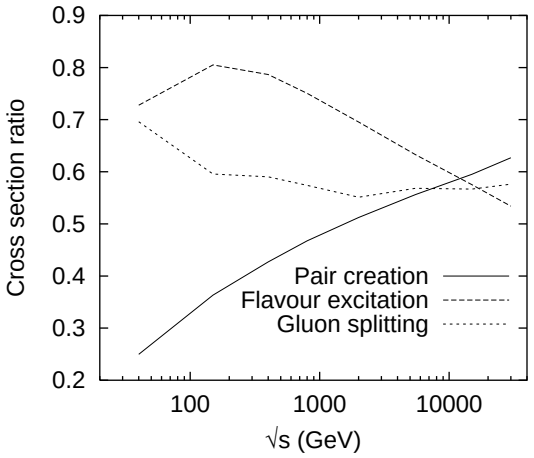

Figure 5: Dependence of the charm cross section on model aspects, for pp collisions as a function of $E_{\mathrm{CM}} = \sqrt{s}$. Shown is the ratio of cross sections: pair creation for $m_{\mathrm{c}} = 1.7$ GeV/$m_{\mathrm{c}} = 1.3$ GeV, flavour excitation for GRV 94L/CTEQ 5L parton distributions, and gluon splitting for $Q^2_{\mathrm{max}} = M^2_{\mathrm{max}} = Q^2/Q^2_{\mathrm{max}} = M^2_{\mathrm{max}} = 4Q^2$.

for gluon splitting, whereas flavour-excitation topologies are more restrictive. At small energies, however, the less demanding kinematical requirements for flavour excitation in a shower gives it an edge over gluon splitting.

The total cross section is strongly dependent on QCD parameters such as the heavy-quark mass, parton distributions, and factorization and renormalization scales. It is not our aim here to present theoretical limits and errors — this has been done elsewhere [13]. However, Fig. 5 gives some examples of how much results may vary. Clearly, the quark-mass choice is very important, especially for charm. Maybe surprisingly, the charm parton distributions in the proton do not differ by that much, probably reflecting a convergence among the common parton distributions and in the scheme adapted for $\mathrm{g} \to \mathrm{Q\overline{Q}}$ branchings in the evolution equations. Among the examples given, the largest uncertainty comes from the choice of the heavy quark mass. However, it should be remembered that the variations above have no formal meaning of a '1σ' range of uncertainty, but merely reflects some more or less random variations.

To gain further insight into the properties of the perturbative production processes, one may study 'non-observables' that characterize the hard-scattering process associated with the production, such as the $\hat{p}_\perp$ of the hard interaction. We also show kinematical distributions, like the rapidity and transverse momentum of the heavy quarks, and correlations between them, in order to quantify in which regions the different production processes contribute. As an example, $\mathrm{b\overline{b}}$ production is studied at a 2 TeV $\mathrm{p\overline{p}}$ collider, where the three production mechanisms are of comparable magnitude. Since the valence-quark-dependent contribution to hard subprocesses is small at this energy, there is no significant difference between pp and $\mathrm{p\overline{p}}$.

Fig. 6 shows the $\hat{p}_\perp$ distribution of the hard interaction, where $\hat{p}_\perp$ is the transverse momentum of the outgoing partons evaluated in the hard-interaction rest frame. The main difference is in the behaviour at small $\hat{p}_\perp$. For the pair creation process, massive LO matrix elements are used, so that $\hat{p}_\perp$ goes all the way down to zero. The differential cross section is not divergent and no explicit $\hat{p}_{\perp\mathrm{min}}$ cut is needed. For the other two processes, massless matrix elements are used as a starting point — implying a divergent cross section in the limit $\hat{p}_\perp \to 0$ — and mass constraints are introduced the back door.

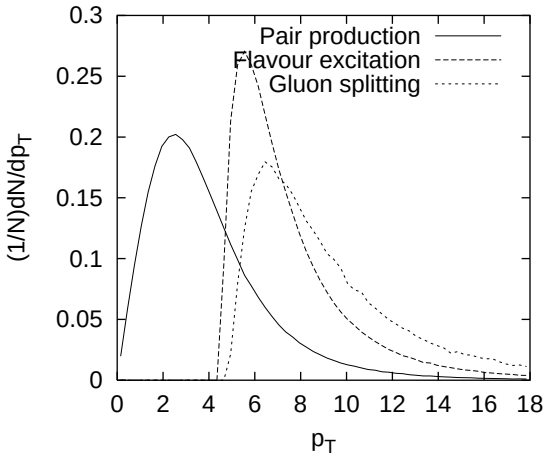

Figure 6: $\hat{p}_\perp$ distributions for the hard interaction associated with a $\mathrm{b\overline{b}}$ event at a 2 TeV $\mathrm{p\overline{p}}$ collider. The pair creation, flavour excitation and gluon splitting curves are each normalized to unit area to simplify comparisons of the shape.

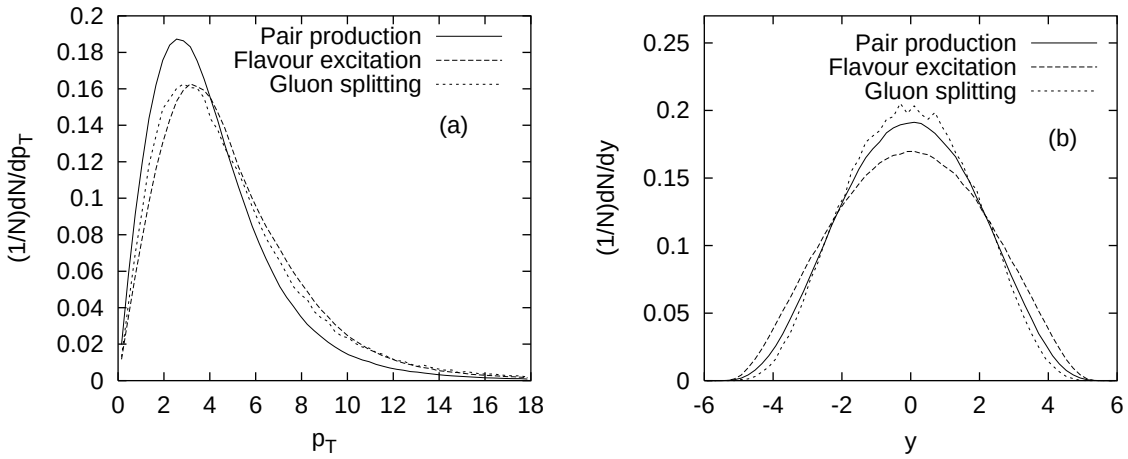

Figure 7: Single $\mathrm{b}/\overline{\mathrm{b}}$ quark (a) $p_\perp$ and (b) y distributions at a 2 TeV $\mathrm{p\overline{p}}$ collider. The curves are each normalized to unit area to simplify comparisons of the shape.

To be able to resolve a heavy quark inside a hadron, i.e. flavour excitation and initial-state gluon splitting, a virtuality $Q^2 = \hat{p}_\perp^2 > m_\mathrm{Q}^2$ is needed, so the quark mass sets $\hat{p}_{\perp\min}$ in this case. (With a massive quark in the final state, the actually reconstructed $p_\perp$ of the hard scattering is always smaller than the nominal $\hat{p}_\perp$ one.) Also the final-state shower contribution to gluon splitting begins at $\hat{p}_{\perp\min} = m_\mathrm{Q}$. Here the shower evolution scale is set by $M^2_\mathrm{max} = 4\hat{p}_\perp^2$, but the threshold for gluon splitting is at $M^2 = 4m_\mathrm{Q}^2$, so the two factors of 4 cancel. We remind that the cuts fill a well-defined function: the heavy-flavour-producing part of the graph cannot be the most virtual one in flavour excitation or gluon splitting, or one would double-count with pair creation. Nevertheless, the very sharp thresholds may be somewhat of an artefact, and are certainly smeared when the effects of further QCD emissions are included.

As an illustration, consider Fig. 7, where we show the single $\mathrm{b}/\overline{\mathrm{b}}$ transverse momentum ($p_\perp$) and rapidity (y) distributions of the produced quarks for the three production channels. Here the full parton-shower and intrinsic-$k_\perp$ smearing effects are included. Now all the $p_\perp$ spectra extend down to $p_\perp = 0$, and the shapes are surprisingly similar,

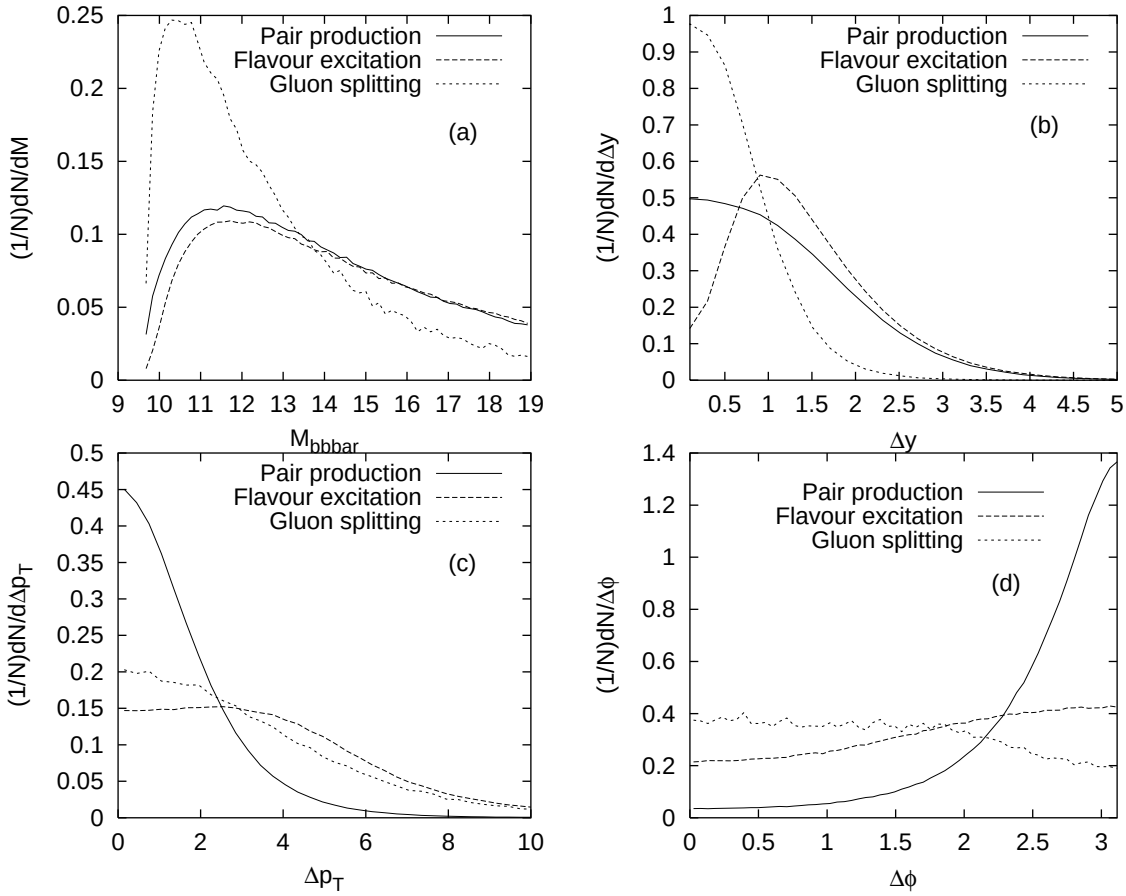

Figure 8: Correlations between b and $\overline{\mathrm{b}}$ at a 2 TeV $\mathrm{p\overline{p}}$ collider: (a) $m_{\mathrm{b\overline{b}}}$, (b) $\Delta y = |y_{\mathrm{b}} - y_{\overline{\mathrm{b}}}|$, (c) $\Delta p_\perp = |p_{\perp\mathrm{b}} - p_{\perp\overline{\mathrm{b}}}|$ and (d) $\Delta\phi = |\phi_{\mathrm{b}} - \phi_{\overline{\mathrm{b}}}|$. The curves are each normalized to unit area to simplify comparisons of the shape.

although pair creation remains somewhat softer than the other two mechanisms. The rapidity spectra agree even better between the three mechanisms, although flavour excitation gives somewhat more production at larger rapidities and gluon splitting more at central ones, as could be expected. This seems to indicate that the heavy-quark production part of the process is more or less independent of what goes on in the rest of the event. There are indeed also similarities in the descriptions, e.g. gluon splitting $\mathrm{g} \to \mathrm{Q\overline{Q}}$ is equivalent to the s-channel graph of pair creation $\mathrm{gg} \to \mathrm{Q\overline{Q}}$, while flavour excitation is closely related to the t-channel graph of pair creation. Furthermore, compensation mechanisms are at play: the $p_\perp$ spectrum of gluon splitting is softened by the Q and $\overline{\mathrm{Q}}$ having to share the $p_\perp$ of the gluon between them, but this is compensated by the relative $p_\perp$ in the $\mathrm{g} \to \mathrm{Q\overline{Q}}$ branching itself.

Correlations between the produced heavy quarks turn out to be more interesting, since here the difference between the three production channels are better visible. In Fig. 8 we present the distributions of $m_{\mathrm{b\overline{b}}}$, $\Delta y = |y_{\mathrm{b}} - y_{\overline{\mathrm{b}}}|$, $\Delta p_\perp = |p_{\perp\mathrm{b}} - p_{\perp\overline{\mathrm{b}}}|$ and $\Delta\phi = |\phi_{\mathrm{b}} - \phi_{\overline{\mathrm{b}}}|$. The invariant mass spectrum is appreciably more peaked for gluon splitting than for the other two mechanisms. Given that gluon splitting is equivalent to the s-channel exchange of a gluon, while the other two are dominated by t-channel contributions, it is clear why the gluon splitting is more suppressed at large $m^2_{\mathrm{b\overline{b}}} =$'$\hat{s}$'. As a logical consequence, also the y correlation is more narrow for gluon splitting.

In the Δy distribution the differences are even more marked. Here flavour excitation

is depleted at small rapidity differences and approaches the pair production spectrum only at large Δy. The explanation of this involves several mechanisms. When a gluon in the parton-distribution evolution splits into a $\mathrm{b\overline{b}}$ pair this gives them a small initial rapidity separation, with a distribution which is centered around zero much like the gluon splitting distribution in Fig. 8b. One of the heavy quarks then enter the hard interaction and is back-scattered by a parton from the other beam. Since the minimum $\hat{p}_\perp$ of the hard interaction here is m_b and this is the largest scale of the process, the rapidity shift can be fairly large. An additional smearing is introduced by further gluon emissions in the parton shower, but not enough to hide the underlying behaviour.

Differences also appear in transverse momentum correlations. In the $\Delta p_\perp$ and $\Delta\phi$ distributions, pair creation is the one most peaked in the region of a heavy-quark pair with opposite and compensating $p_\perp$. Thus the basic LO-process behaviour largely survives showers and primordial $k_\perp$. In the other two processes the correlations are more smeared. Especially discerning is the $\Delta\phi$ distribution, where gluon splitting gives an almost flat curve, pair creation a clear peak near 180°, and flavour excitation is somewhere in between. In gluon splitting, the $p_\perp$ of the hard scattering favours small angles and the $p_\perp$ of the splitting itself large angles, so the near-flat curve is the result of a non-trivial balance. Needless to say, a cut on the $p_{\perp\mathrm{b}}$ and $p_{\perp\overline{\mathrm{b}}}$ values would distort the $\Delta\phi$ distribution significantly: at large $p_\perp$'s, pair creation becomes more peaked at large angles and gluon splitting peaked at small angles.

To summarize, we note that flavour excitation and gluon splitting give significant contributions to the total heavy quark cross section at large energies and thus must be considered. NLO calculations probably do a better job on the total b cross section than the shower approach, whereas for the lighter c quark, production in parton showers is so large that the NLO cross sections are more questionable. The shapes of single heavy quark spectra are not altered as much as the correlations between Q and $\overline{\mathrm{Q}}$ when flavour excitation and gluon splitting is added to the leading order result. Similar observations have been made when comparing NLO to LO calculations [12, 35].

3.2 Properties of the fragmentation

We now proceed to describe properties of the fragmentation process. In the Lund string fragmentation model no new heavy flavours are produced during the fragmentation, so the model can 'only' map the momentum of a heavy quark onto the momentum and species of a heavy hadron in the final state. This can, however, be dramatic enough, e.g. with hadrons formed at larger momenta than the perturbatively produced quark, or with flavour asymmetries favouring the production of heavy hadrons sharing light valence quark flavours with the incoming beam particles. Such topics will be covered in detail in the following section, so here we only mention a few of the basic aspects.

The fate of a colour singlet system in the string model depends on its mass and on its flavour content. The mass spectrum of strings/clusters containing one heavy flavour and a u or d quark at the other end is shown in Fig. 9 for two typical processes. Here we are only interested in the low-mass behaviour where only few primary hadrons are produced. (Secondary decays, of everything from ρ to B^*, is not considered here.) In the high mass region traditional string fragmentation should work well. Technically, the description is split into clusters, giving one or two hadrons, and strings, giving two or more. In total, the area under the curve in Fig. 9 splits into these four contributions. The transition from one to two hadrons comes in a set of steps, somewhat smeared e.g. by the ρ Breit-Wigner

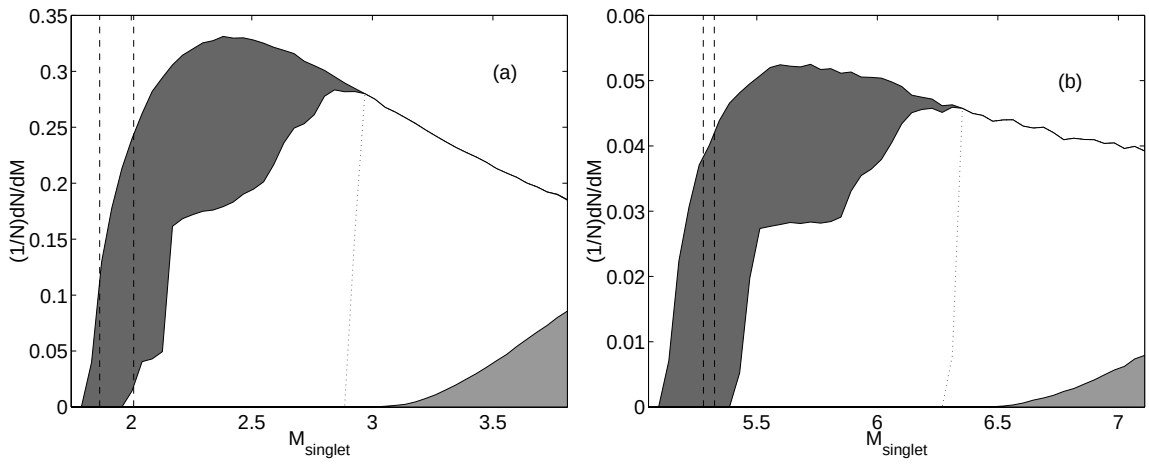

Figure 9: The fate of a cluster/string as a function of its mass, (a) for charm in π^-p collisions with a π^- beam momentum of 500 GeV, and (b) for bottom in $\mathrm{p\overline{p}}$ collisions at 2 TeV. The full curve represents the original mass spectrum, for simplicity only from pair creation. Clusters within the gray area to the left collapse to a single particle, predominantly the D/D* or B/B* states indicated by dashed vertical lines. The white middle area gives two primary hadrons, with cluster decay to the left of the dotted curve and with string fragmentation to the right. The rightmost gray area corresponds to the production of three or more primary hadrons from the string.

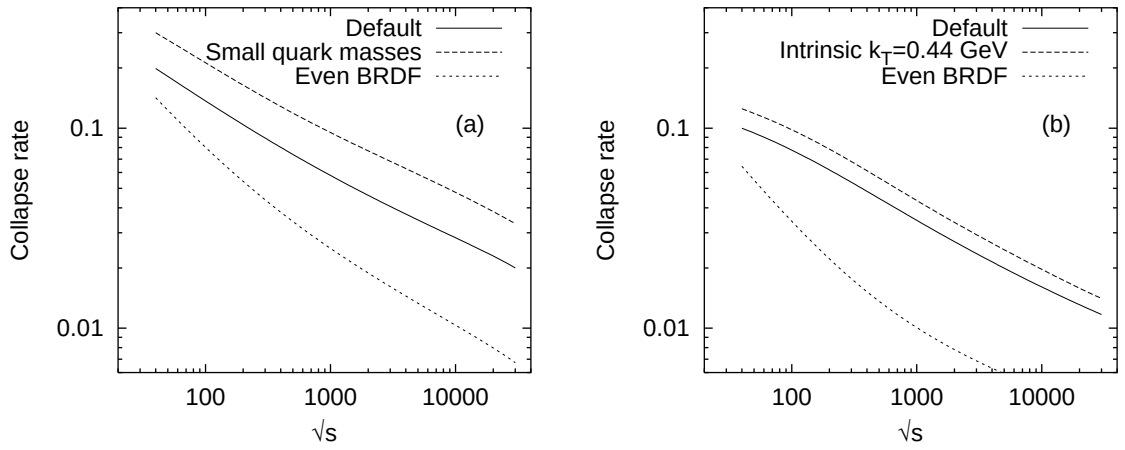

Figure 10: The average number of cluster collapses to a single heavy hadron per heavy-quark event, for (a) charm and (b) bottom in a pp collision as a function of $E_{\mathrm{CM}} = \sqrt{s}$. For simplicity, only pair creation is included.

shape. That from two to three particles is continuous, but still slightly tailor made. Only beyond that is the multiplicity determined fully dynamically, by fragmenting off hadrons of random energies until all has been used up.

The mass spectrum near threshold, and thus the amount of collapses to a single hadron, is sensitive to a large number of parameters, such as the heavy and light quark/diquark masses, the average primordial $k_\perp$, and the beam-remnant description [10]. Some of these are constrained by information from other processes, but a significant uncertainty remains. By introducing some piece of experimental data, such as the flavour asymmetries in π^-p collisions, a reasonable overall set of parameters has been found. The energy dependence

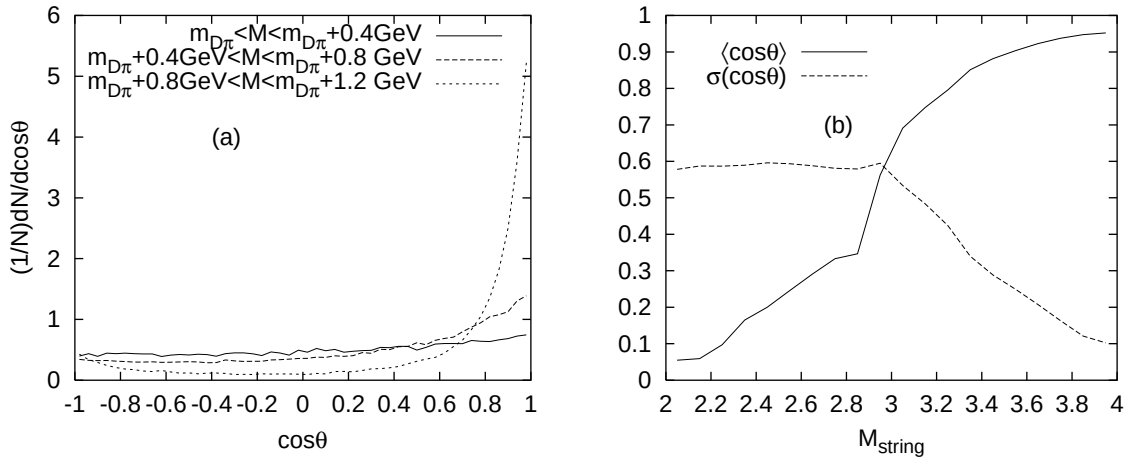

Figure 11: Direction of a D/D* hadron in the decay of a $\mathrm{c\overline{d}}$ string/cluster at rest. (a) The distribution $\mathrm{d}n/\mathrm{d}(\cos\theta)$, with θ the angle between the c and D/D*, for a few masses. (b) $\langle\cos\theta\rangle$ and $\sigma(\cos\theta)$ as a function of the string/cluster mass.

of the collapse rate is then predicted, Fig. 10. The drop with larger energies is a natural consequence of the string mass spectrum then extending to larger values. The collapse rate can be shifted up or down e.g. by varying the charm mass, and shifted in shape by the beam-remnant description, but always follows the same qualitative behaviour. No input has been used from B physics, so here measurements would directly test the universality of the model. Note that the collapse rate is expected to be lower for bottom than for charm, since the mass spectrum near threshold scales roughly with m/m_{Q}, i.e. the bulk of the mass spectrum is higher above threshold for heavier quarks, while the upper limit for collapse goes like m_{Q}+constant.

The transition between the cluster and string two-hadron scenarios is purely artificial, and in the best of worlds the treatments should smoothly match at the crossover. In the new PYTHIA version, an attempt has indeed been made to ensure that. Specifically, the cluster decays anisotropically in a fashion that should mimic the string scheme for the larger cluster masses. We have studied the angular distributions in the transition region and found this to be reasonably well fulfilled, Fig. 11.

When a cluster collapses to a single hadron, energy and momentum is redistributed between this system and the rest of the event. The mass shift in the collapsing cluster is implicit in the shape of the leftmost gray area in Fig. 9, and an explicit illustration is given in Fig. 12a. With the current default set of quark masses and form of the two-particle threshold, it is more likely that the produced hadron has a smaller mass than the original cluster. For lower quark masses, it is possible to reverse this asymmetry, but then at the price of a cluster collapse rate in excess of what is indicated by data. The string system that takes the energy/momentum recoil of the collapse clearly will see its mass shifted in the opposite direction, Fig. 12b. If the cluster and string are at relative rest, the two mass shifts are exactly compensating, but a relative motion tends to distort this, in the direction of a larger (opposite) string mass shift than cluster mass shift. The reasonably narrow distribution in Fig. 12b then indicates that the compensation algorithm is working well.

The colour connection between the produced heavy quarks and the beam remnants in the string model gives rise to an effect called beam remnant drag. In an independent fragmentation scenario, a quark jet fragments symmetrically around the quark direction. The

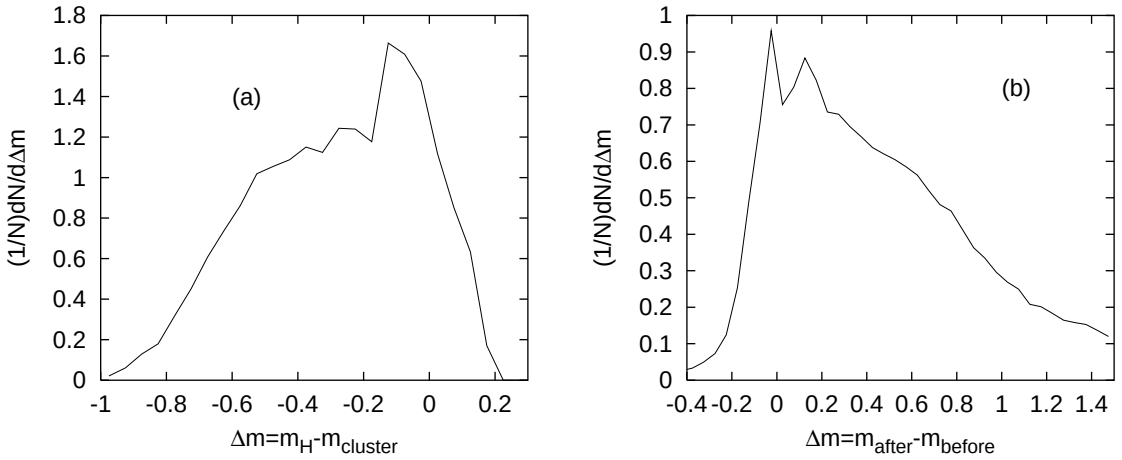

Figure 12: Distribution of mass shifts induced by the collapse of clusters to a single charm hadron, in π^-p collisions with a π^- beam momentum of 500 GeV, and for simplicity only including pair creation. (a) For the collapsing system, i.e. $\Delta m = m_{\mathrm{H}} - m_{\mathrm{cluster}}$. (b) For the string taking the momentum recoil, $\Delta m = m_{\mathrm{after}} - m_{\mathrm{before}}$.

light cone (along the quark axis) energy-momentum of the quark is then simply scaled by some factor, picked from a fragmentation function, in order to give the momentum of the hadron. Thus, on average, the rapidity would be conserved in the fragmentation process. This is not necessarily so in string fragmentation where both string ends contribute to the four-momentum of the produced heavy hadron. If the other end of the string is a beam remnant, the hadron will be shifted in rapidity in the direction of the beam remnant, often resulting in an increase in $|y|$. This beam-drag is shown qualitatively in Fig. 13, where the rapidity shift for bottom hadrons in a 2 TeV $\mathrm{p\overline{p}}$ collision is shown as a function of rapidity and transverse momentum. We use two different measures of the rapidity shift. The first is the average rapidity shift $\Delta y = \langle y_{\mathrm{B}} - y_{\mathrm{b}} \rangle$. Here the heavy quark can be connected to a beam remnant on either side of the event, giving rise to shifts in both directions which tend to cancel in inclusive measures. A better definition is therefore

$$\Delta y_{\mathrm{sign}} = \langle (y_{\mathrm{B}} - y_{\mathrm{b}}) \cdot \mathrm{sign}(y_{\mathrm{other\ end}}) \rangle, \tag{12}$$

which measures the rapidity shift in the direction of the other end of the string. This shift should almost always be positive. The rapidity shift is not directly accessible experimentally, only indirectly as a discrepancy between the shape of perturbatively calculated quark distributions and the data.

3.2.1 High-$p_\perp$ asymmetries

There is another possible asymmetry which occurs at large transverse momentum, involving the collapse and drag of scattered valence quarks and heavy quarks produced by gluon splitting in the parton shower. As an illustration, consider Fig. 14 where a valence u quark is scattered to high transverse momentum in a high energy pp collision. In such high-$p_\perp$ jets, parton showering will be profuse. If a gluon close to the scattered u quark splits into a heavy quark pair, the heavy antiquark could be in a colour singlet system together with the scattered u quark. If this singlet has a small mass it could collapse into a single heavy hadron. Heavy hadrons with its light quark constituent in common with the beam will thus be favoured. The effect then is due to the asymmetry in the composition of jet

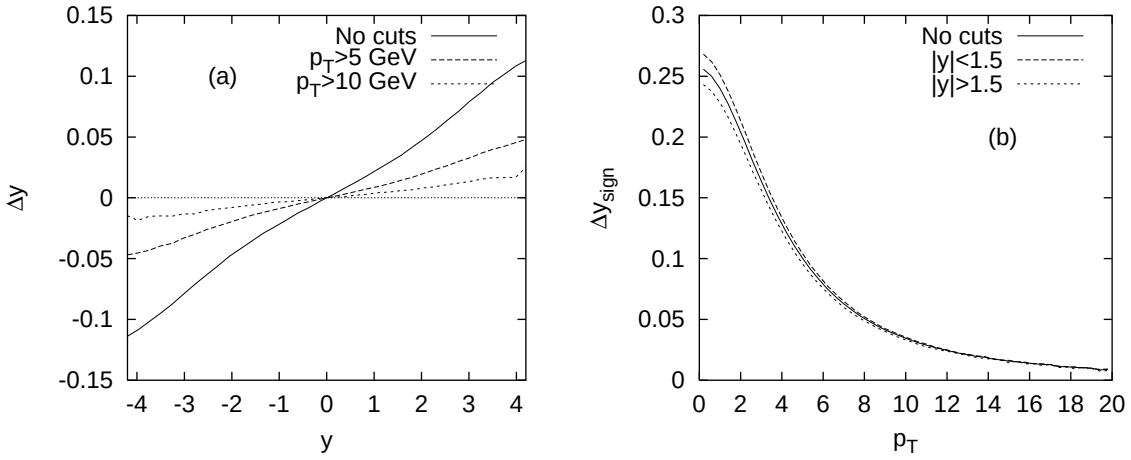

Figure 13: (a) Average rapidity shift Δy as a function of y for some different $p_\perp$ cuts for a $\mathrm{p\overline{p}}$ collider at 2 TeV. (b) Average rapidity shift Δy_{sign} as a function of $p_\perp$ for some different rapidity cuts.

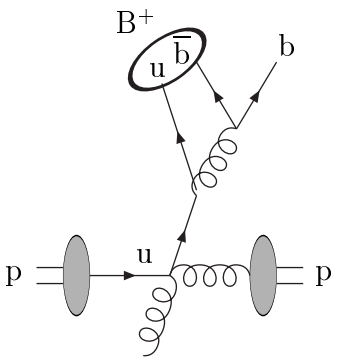

Figure 14: Illustration of the high-$p_\perp$ asymmetry.

flavours. At reasonably low $p_\perp$, where gluon (and second to that seaquark) jets dominate, effects therefore are vanishingly small.

This mechanism was studied in [36] and the size of the effect was found to be at the 10^{-3} level. Here we would like to study if the modifications to the model has changed this result. To increase the effectiveness we study high-$p_\perp$ quark jets in a 14 TeV pp collision and look at B mesons produced within the jets. To be specific, and hint at a possible experimental procedure to study the effect, we generate events containing the subprocess $\mathrm{qq'} \to \mathrm{qq'}$ (where q is a scattered valence quark) with $\hat{p}_{\perp,min} > 500$ GeV and look for events containing two high-$p_\perp$ jets. We use a cone algorithm to find the jets and then look for B mesons within these jets which carry at least 20% of the jet $E_\perp$. The asymmetry between $\mathrm{B^0}$ and $\mathrm{\overline{B}^0}$ fulfilling these criteria was found to be 0.019 ± 0.005 and the asymmetry between $\mathrm{B^+}$ and $\mathrm{B^-}$ 0.011 ± 0.005. The size of possible collapse asymmetries is limited by the probability for a b hadron within a jet to be produced in a collapse between a scattered valence quark and a b quark. This probability was found to be at the 10^{-3} level. This indicates that another mechanism is at play giving rise to a larger asymmetry. Furthermore, the two asymmetries above might have been expected to be of opposite sign, by equality between the number of b and $\mathrm{\overline{b}}$ quarks, at least if strangeness and baryon production can be neglected.

A possibility is that gluon splittings on the perimeter of the jet-cone give rise to $\mathrm{b\overline{b}}$ pairs where the $\overline{\mathrm{b}}$ is colour connected to the scattered valence quark and the b is connected to the beam remnant diquark. In the string fragmentation process the $\overline{\mathrm{b}}$ could be dragged towards the scattered high-$p_\perp$ quark at the center of the jet and the b towards the low-$p_\perp$ beam remnant, i.e. away from the jet, thus lowering the rate of $\overline{\mathrm{B}}^0$ and B^- within the jet and at the same time giving rise to a slightly harder $p_\perp$ spectrum for leading B mesons at high $p_\perp$. This is simply a variation of the drag effect already discussed, only this time the drag is in the transverse direction instead of the longitudinal one.

The total asymmetry then is a convolution of the asymmetry in the composition of jet flavours with the asymmetry in the b hadronization mechanisms. To get an estimate of the total asymmetry the result above must be diluted with all other non-asymmetry-generating QCD processes contributing to high-$p_\perp$ jets containing B mesons, e.g. $\mathrm{gg} \to \mathrm{gg}$ and flavour excitation. The ratio between the cross sections for producing a B meson within a valence quark jet and within any jet is approximately 0.035 in this specific case, so the diluted $\mathrm{B}^0/\overline{\mathrm{B}}^0$ asymmetry is $(6.5 \pm 1.7) \cdot 10^{-4}$. The lesson to be learned is that asymmetries can turn up also when not expected and will depend on the procedure used in studying the effects, like jet $p_\perp$, jet clustering algorithms, and B hadron selection criteria.

4 Applications

In this section we apply the model presented in the preceding sections to some typical current and future experiments at both small and large energies. No attempt will be made to be exhaustive, instead different examples will be picked as illustrations of the basic ideas. At low energies the most striking effect is the flavour asymmetries already observed in several experiments [4, 5, 6, 7, 8]. At large energies the most important aspect may be the beam drag effect, suggested in HERA data both for photoproduction [37] and deep inelastic scattering (DIS) [38].

Since the model is available in Monte Carlo form, further studies are left to the interested reader. However, there are some caveats. In particular, nuclear-target effects are not simulated. Instead such a target has to be represented by a single proton or neutron, with total cross sections suitably rescaled. One does not expect large nuclear effects in the heavy-flavour production characteristics, but effects may be non-negligible.

4.1 Fixed-target π^-p

Charm production in fixed-target π^-p collisions was already studied in [10, 42], but only using the pair creation mechanism of charm production. Here we will extend the results to the other production mechanisms and to correlations between the two charm hadrons in the event.

We see from Fig. 4 that gluon splitting does not give a significant contribution to the total charm cross section for fixed-target energies around 30 GeV. Flavour excitation, on the other hand, gives a contribution to charm production which is as large as the pair production one even at these low energies. Fig. 15 shows the single heavy hadron x_F and $p_\perp^2$ distributions as predicted by the model, using the default parameters, compared to data from the WA82 [5] and WA92 [6] experiments. The leading order pair creation result and the result with all production channels added together are shown separately. The agreement with data is reasonable, though the x_F spectra are slightly harder than the data, especially for D^+ which is non-leading. The resulting asymmetry as a function

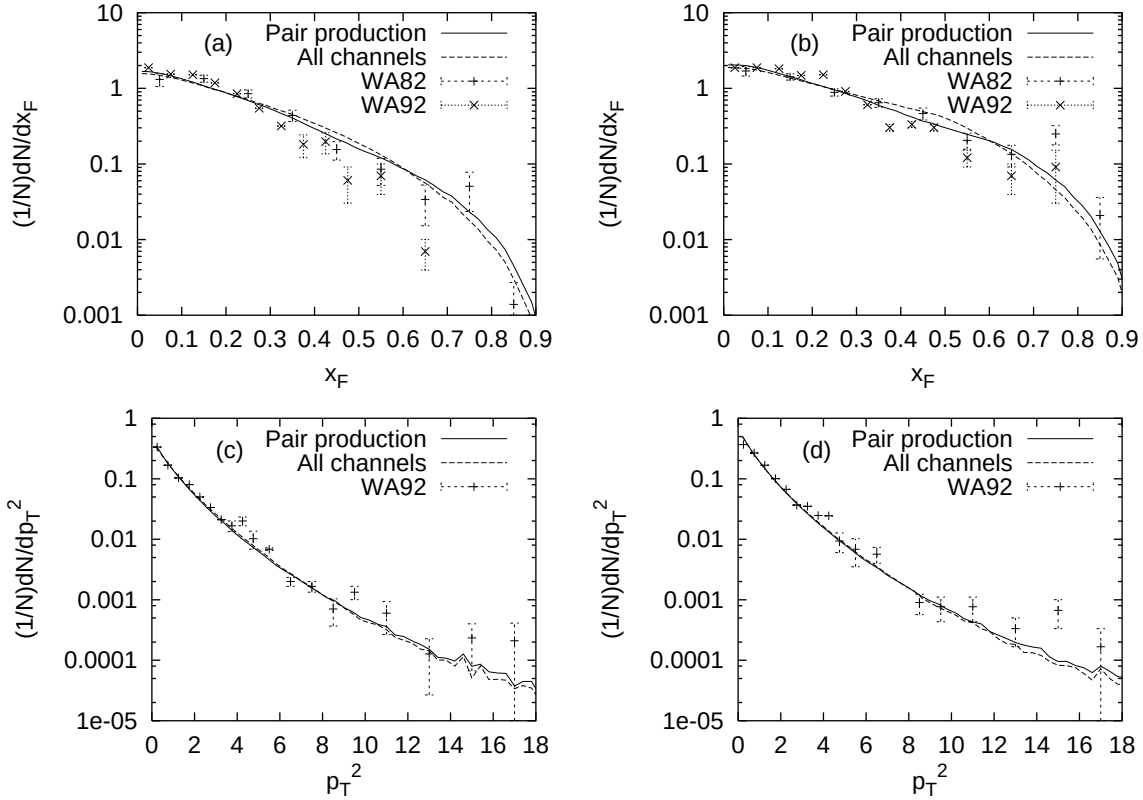

Figure 15: D^+/D^- meson spectra in a π^-p collision with $\sqrt{s} = 26$ GeV. (a) Single D^+ x_F distributions. (b) Single D^- x_F distributions. (c) Single D^+ $p_\perp^2$ distributions. (d) Single D^- $p_\perp^2$ distributions. The distributions are normalized to the sum of the experimental D^+ and D^- cross sections in each case.

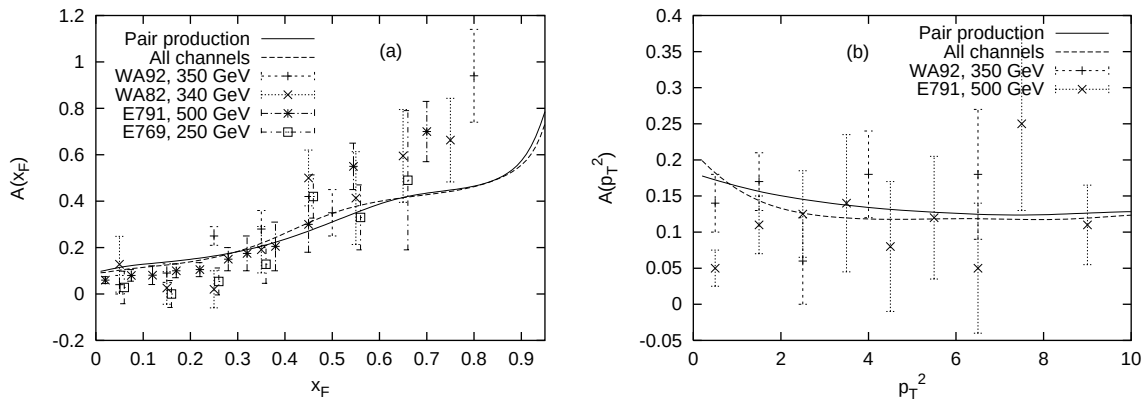

Figure 16: The resulting asymmetry as a function of x_F and $p_\perp^2$. The theoretical curves are model results for a 340 GeV π^- beam on a proton target ($\sqrt{s} = 26$ GeV).

of x_F and $p_\perp^2$ is shown in Fig. 16. The data are taken at slightly different energies but the energy dependence of the model is small within the experimental energy range. This seems to be true also for the data. As expected from the study in Sec. 3.1, single charm spectra and asymmetries are not significantly altered by the addition of flavour excitation and gluon splitting.

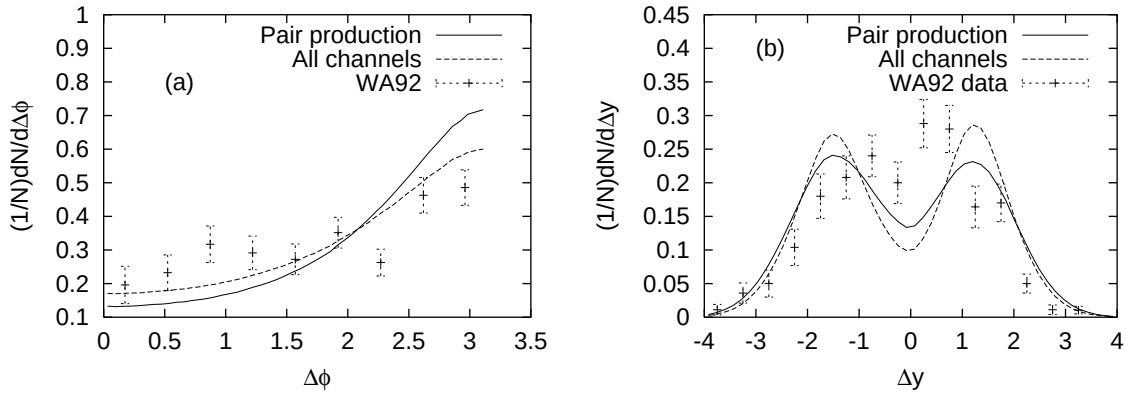

Figure 17: Correlations between D^+ and D^- when at least one D meson is produced with $x_F > 0$ for a π^-p collision with $\sqrt{s} = 26$ GeV. The figure shows the distribution of (a) $\Delta\phi = |\phi_{D^+} - \phi_{D^-}|$ and (b) $\Delta y = y_{D^+} - y_{D^-}$. The distributions are normalized to the total D^+D^- cross section in each case. The data is taken from the WA92 experiment [39].

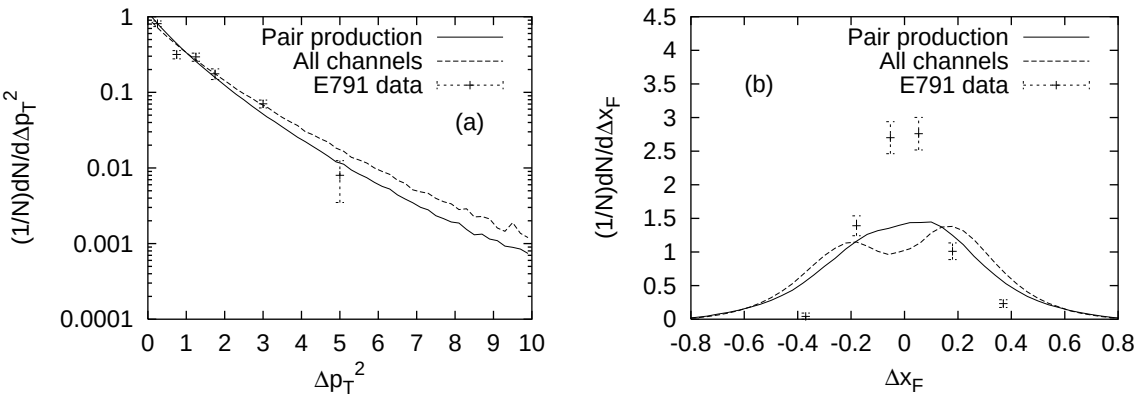

Figure 18: Correlations between D and $\overline{\mathrm{D}}$ mesons when both are produced with rapidity $-0.5 < y < 2.5$ for a π^-p collision with $\sqrt{s} = 30$ GeV. The figure shows the distribution of (a) $\Delta p_\perp^2 = |p_{\perp,\mathrm{D}}^2 - p_{\perp,\overline{\mathrm{D}}}^2|$ and (b) $\Delta x_F = x_{F,\mathrm{D}} - x_{F,\overline{\mathrm{D}}}$. The distributions are normalized to the total $\mathrm{D}\overline{\mathrm{D}}$ cross section in each case. The data is taken from the E791 experiment [40].

Fig. 17 shows the correlation in ϕ, the angle between D^+ and D^- in the transverse direction, and rapidity, y compared to data from the WA92 experiment [39]. The model prediction for correlations is more sensitive to the addition of flavour excitation and gluon splitting than single charm spectra are, again as expected from Sec. 3.1. In this case the description of data is improved for the transverse correlation ($\Delta\phi$) but not for the longitudinal (Δy) one. The large separation in the rapidity distribution is a consequence of the colour connection between the produced charm quarks and the beam remnants, which tend to shift the charm momenta in the direction of the respective beam remnant, thus increasing the rapidity separation. The same pattern is repeated when comparing correlation distributions to the E791 collaboration [40] in Fig. 18.

There are two mechanisms which could decrease the rate of connection. The first is gluon splitting into light quarks ($g \to q\overline{q}$) in the parton shower and the other is

	$\frac{\sigma(D^+,D^-)}{\sigma(D^0,\overline{D}^0)}$	$\frac{\sigma(D_s^+,D_s^-)}{\sigma(D^0,\overline{D}^0,D^+,D^-)}$	$\frac{\sigma(D^-)}{\sigma(D^+)}$	$\frac{\sigma(D^0)}{\sigma(\overline{D}^0)}$
Model	0.33	0.11	1.39	0.94
Experimental average [6]	0.415	0.129	1.35	0.93

Table 1: Cross section ratios for π^-p collisions around 26 GeV.

colour reconnections [33, 34]. Gluon splitting would split the string in two and each would then hadronize independently. The memory of the colour connection is decreasing for each splitting of the string, thus decreasing the drag in the direction of the beam remnants. However, at these low energies the phase space for gluon splitting is limited. Colour reconnection by soft gluon exchange could change the colour structure of the event, thus making the charm quark lose its colour connection to the beam remnant. In the simplest scenario the charm quark pair could be reconnected to form a $c\overline{c}$ colour singlet, causing them to pull each other closer, resulting in a drastic decrease in $\langle \Delta y \rangle$. However, this mechanism would increase the production of J/ψ from collapses of low-mass $c\overline{c}$ colour singlet systems. Given the experimental ratio of J/ψ to $D\overline{D}$ production, $\sigma(J/\Psi)/\sigma(D\overline{D}) \sim 0.02$ [41], and a collapse probability of $\sim$50% in reconnected events (not all to J/Ψ), the colour reconnection probability would thus be limited to 5 – 10 %. More complicated colour reconnections could be imagined, involving also gluons from the parton shower, where the charm quarks are not always in a colour singlet but still not connected directly to the beam remnants. This kind of more sophisticated colour reconnection models have been used with some success to describe J/ψ production and rapidity gaps in hadronic collisions and DIS [34]. The colour reconnection rates needed to describe the longitudinal correlations would also significantly soften the single charm distributions as well as lower the asymmetry. This is not favoured by the data so in the following we only consider single heavy quark distributions which are well described by the model.

We also compare results on some cross section ratios shown in Table 1 and again the description is reasonable but not perfect. The cross sections are interrelated by several model aspects. Consider e.g. the ratio of D_s to D_q. The main parameter that determines the rate of strangeness production in the fragmentation is the ratio between u, d and s production, which by default is set to 1:1:0.3. This number has been fitted to e^+e^- data and can not be changed appreciably. The D_s production ratio is also sensitive to the collapse rate of colour singlets containing charm and a light quark from a beam remnant. A large collapse rate decreases the ratio, because D_s is depleted in favour of D_q when the beam consists of non-strange particles (like in this case π^-).

To summarize, we find good agreement with several fixed target experiments when it comes to single charm spectra and asymmetries. The only case where the model does not perform well is for longitudinal correlations. Similar results were obtained [42] in comparisons with the E791 experiment [40]. In that study the contradiction between single charm and correlation data from different experiments was observed, a problem that as of yet has not been resolved, as we have seen.

4.2 HERA-B

The HERA-B experiment at DESY is a fixed-target experiment built especially for bottom studies. The experiment will study pA collisions at a center of mass energy of about 40

GeV. It is therefore an ideal experiment to test the results of Section 4.1 for bottom quarks. Predictions for $B\overline{B}$ asymmetries and spectra follow directly from the model using the new updated set of parameters and hadronization mechanisms. The HERA-B experiment collides protons with nuclei but we do not include any simulation of nuclear effects. We take into account the neutrons in the nuclei by simulating pp and pn events separately and use the mean to produce the plots. The only missing pieces are then the bottom quark mass and the proton beam remnant distribution. By the simple ansatz of eq. (3) we obtain $m_{\rm b} = 4.8$ GeV. The BRDF of the proton is more problematic because there is no fundamental understanding of its structure. There are some indications that an even sharing of energy-momentum is favoured by experiments [8, 43]. We have tried different parameterizations but found no significant qualitative differences (see e.g. Fig. 19).

Fig. 19 shows the distribution of bottom mesons at HERA-B, showing both the size of the drag effect and asymmetries. The asymmetry is significant at all rapidities, not only large ones, and can reach as high as 20% even in the central rapidity region. When the kinematical limit at large rapidities is approached, the asymmetry changes sign for small $p_\perp$ because of the drag-effect; b quarks connected to diquarks from the proton beam remnant which carry most of the remnant energy often produce $\overline{\rm B}^0$ hadrons which are shifted more in rapidity than the $\rm B^0$'s are. Cluster collapse, on the other hand, tend to enhance the production of 'leading' particles (in this case $\rm B^0$) so the two mechanisms give rise to asymmetries with different signs. Collapse is the main effect at central rapidities while eventually at very large y, the drag effect dominates. This is also reflected in the $p_\perp$ dependence of the asymmetry which exhibits a sign shift at small $p_\perp$. The $p_\perp$ dependence is, however, partly a consequence of the fact that large $p_\perp$'s imply small $|y|$. Compared to pp, the asymmetry is slightly larger for pn collisions in the negative rapidity region. This is a natural consequence of the larger amount of d quarks in the neutron beam remnant.

4.3 The Tevatron Collider

The Tevatron $\rm p\overline{p}$ collider operating at CM energies up to 2 TeV represent a significant step up the energy ladder and offers a good opportunity to check the energy dependence of our results. We first show some generic distributions for the Tevatron and then consider a scenario where very forward, low-$p_\perp$ bottom hadrons can be detected. We use $2.5 < |y| < 4$ and $p_\perp < 5$ GeV. This would be ideal for studying the drag effect which is inherently a low-$p_\perp$/high-y phenomenon, see Fig. 13.

Fig. 20 shows the distribution of bottom quarks and the hadrons produced from them, as well as the asymmetry between $\rm B^0$ and $\overline{\rm B}^0$ without any kinematical cuts. The trend is similar to that of HERA-B, but the asymmetry is antisymmetric because of the asymmetry of the initial state. Therefore the asymmetry is zero at y=0 and increasing in different directions for increasing/decreasing rapidities. As expected from Fig. 10, the integrated asymmetry has decreased significantly.

In Fig. 21 we introduce cuts in order to study the region of large rapidities and small $p_\perp$. $\overline{\rm B}^0$ is shifted slightly more in the direction of the beam remnant than $\rm B^0$, but the size of the effect is quite small, approaching 4% at very large rapidities. Still, if large precision is desired in CP violation studies, this effect could be non-negligible.

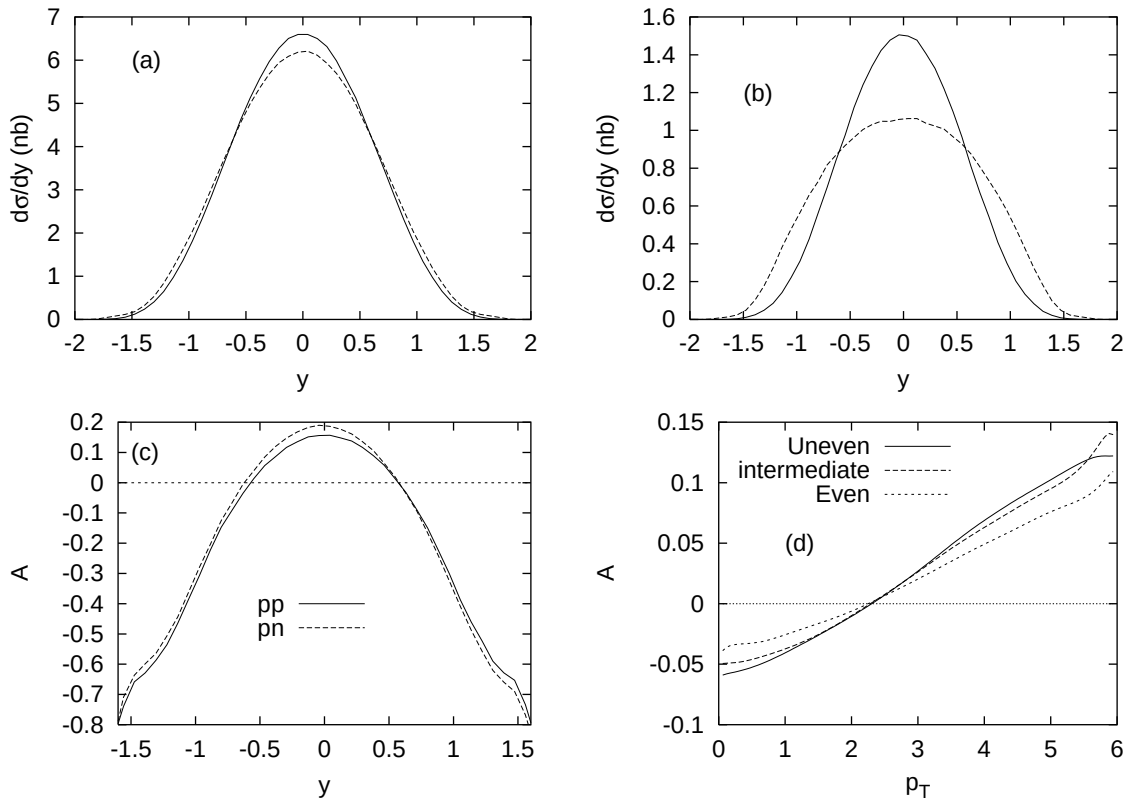

Figure 19: Bottom production in a pA collision at HERA-B energies, neglecting nuclear effects. (a) Rapidity distribution of bottom quarks (full) and the B hadrons produced from them (dashed). (b) Rapidity distribution of B^0 (full) and $\overline{B}^0$ (dashed). (c) The asymmetry $A = \frac{\sigma(B^0)-\sigma(\overline{B}^0)}{\sigma(B^0)-\sigma(\overline{B}^0)}$ as a function of rapidity comparing pp and pn collisions. (d) The asymmetry as a function of $p_\perp$ for three different parameterizations of the BRDF of the proton. For simplicity, only pair production is included.

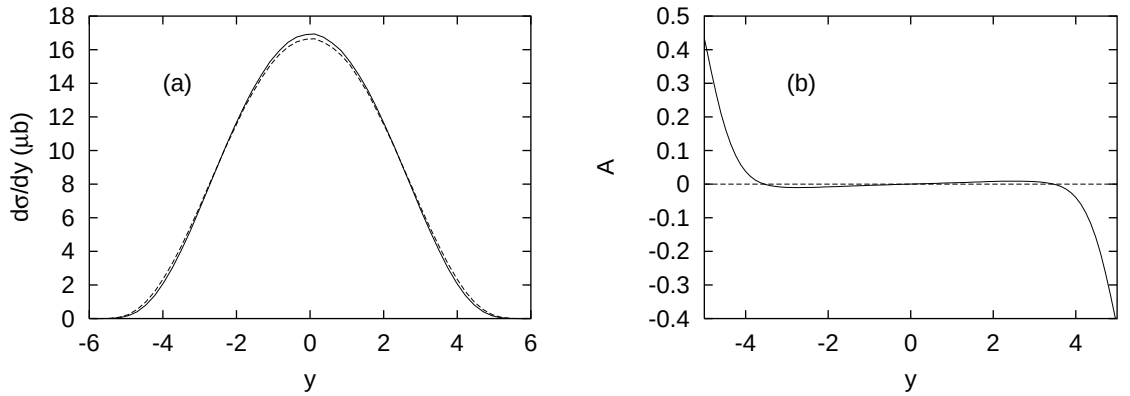

Figure 20: Bottom production at the Tevatron. (a) Rapidity distribution of bottom quarks (full) and the B hadrons produced from them (dashed). (b) The asymmetry $A = \frac{\sigma(B^0)-\sigma(\overline{B}^0)}{\sigma(B^0)-\sigma(\overline{B}^0)}$ as a function of rapidity. For simplicity, only pair production is included.

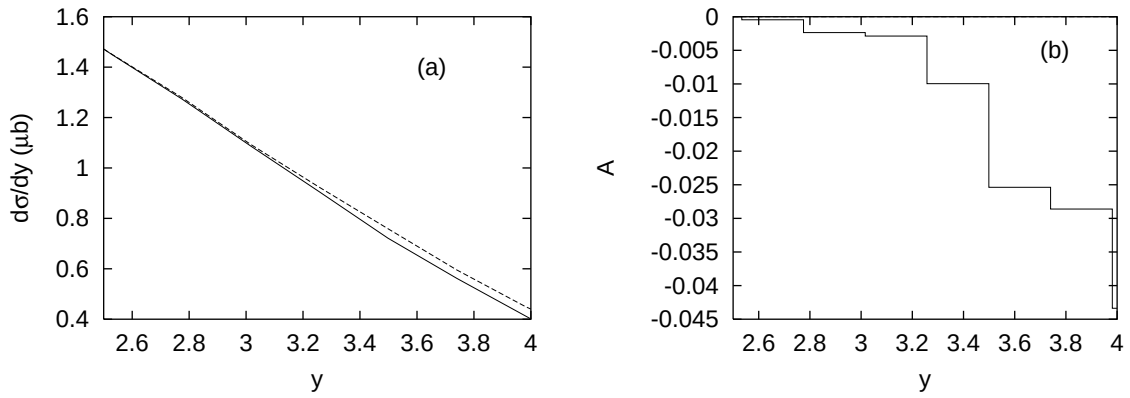

Figure 21: Bottom production at the Tevatron for $2.5 < |y| < 4$ and $p_\perp < 5$ GeV. (a) B^0 (full) and $\overline{B}^0$ (dashed) rapidity spectra. (b) The asymmetry $A = \frac{\sigma(B^0)-\sigma(\overline{B}^0)}{\sigma(B^0)-\sigma(\overline{B}^0)}$ as a function of rapidity. For simplicity, only pair production is included.

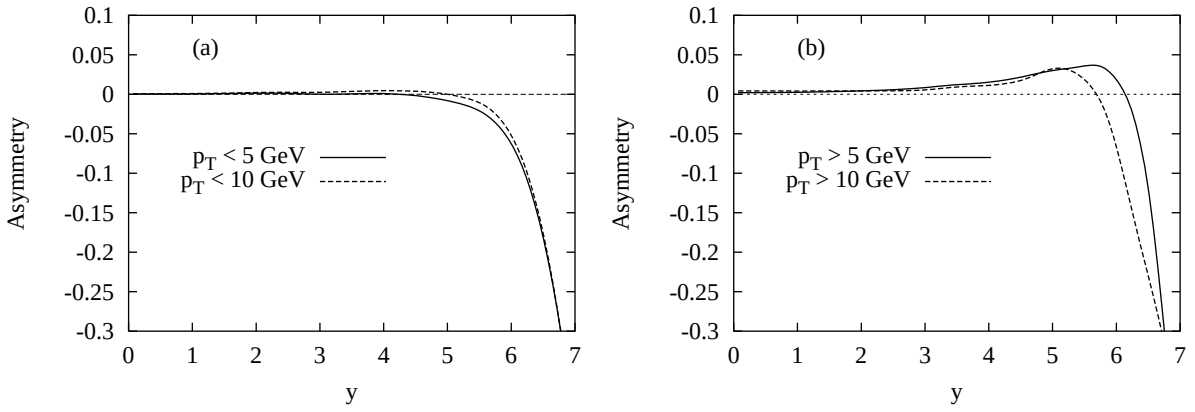

Figure 22: The LHC asymmetry, $A = \frac{\sigma(B^0)-\sigma(\overline{B}^0)}{\sigma(B^0)+\sigma(\overline{B}^0)}$, as a function of rapidity for different $p_\perp$ cuts: (a) $p_\perp < 5, 10$ GeV and (b) $p_\perp > 5, 10$ GeV using parameter set 1 as described in the text. For simplicity, only pair production is included.

4.4 LHC

The difference between the Tevatron and the LHC collider is mainly that the energy at the LHC is one order of magnitude larger and both colliding particles are protons. Due to the similarities we only give some generic results on asymmetries and try to assess the theoretical uncertainty of the model by looking at some parameter variations.

Fig. 22 shows the asymmetry between B^0 and $\overline{B}^0$ as a function of y for several $p_\perp$ cuts in the string model. The asymmetry is essentially zero for central rapidities, where the beam remnant flavour content is not felt so much. At intermediate rapidities it is then positive (except at small $p_\perp$) only to turn negative at larger rapidities. The reason is the same as for HERA-B, but here the switch over is closer to the kinematical limit at large rapidities.

In Table 2 we study the parameter dependence of the asymmetry by looking at the integrated asymmetry for different kinematical regions using three different parameter sets:

Parameters	$\|y\| < 2.5$, $p_\perp > 5$ GeV	$3 < \|y\| < 5$, $p_\perp > 5$ GeV	$\|y\| > 3$, $p_\perp < 5$ GeV
Set 1	0.003(1)	0.015(2)	−0.008(1)
Set 2	−0.000(2)	0.009(3)	−0.005(2)
Set 3	0.013(2)	0.020(3)	−0.018(2)

Table 2: Parameter dependence of the asymmetry in the string model. The statistical error in the last digit is shown in parenthesis (95% confidence). For simplicity, only pair creation is included.

- **Set 1** is the new default as described in Sec. 2.
- **Set 2** The same as Set 1 except it uses simple counting rules in the beam remnant splitting, i.e. each quark get on average one third of the beam remnant energy-momentum.
- **Set 3** The old parameter set, before fitting to fixed-target data, is included as a reference. This set is characterized by current algebra masses, lower intrinsic $k_\perp$, and an uneven sharing of beam remnant energy-momentum.

We see that in the central region the asymmetry is generally very small whereas for forward (but not extremely forward) rapidities and moderate $p_\perp$ the asymmetry is around 1–2%. In the very forward region at small $p_\perp$, drag effects dominates, which can be seen from the change in sign of the asymmetry. The asymmetry is fairly stable under moderate variations in the parameters even though the difference between the old and new parameter sets (Set 1 and 3) are large in the central region. Set 1 typically gives rise to smaller asymmetries. Note also that asymmetries on the perturbative level, calculated to NLO [12], could become relatively more important at LHC energies, where the collapse asymmetries are small. Other non-perturbative effects, such as intrinsic bottom, are also expected to be small at LHC energies [44].

To summarize, we find small asymmetries at the LHC except at large rapidities. Unless the other b in the event is unambiguously tagged, the asymmetry is still not completely negligible for high-precision CP asymmetry studies, especially at LHC-B.

4.5 Photoproduction

The model can also be used in the photoproduction of heavy quarks in γp collisions. Here we wish to apply the model to γp physics at HERA. The asymmetries are small in this case because of the high energy and the flavour neutral photon beam. Instead we study beam-drag effects, consequences of the photon structure and higher-order effects.

The photon is a more complicated object than a hadron because it has two components, one *direct* where the photon interacts as a whole and one *resolved* where it has fluctuated into a $q\overline{q}$ pair before the interaction. This will result in very different event structures in the two cases. This study is constrained to real photons (photoproduction) as modeled by Schuler and Sjöstrand [45] and implemented in the PYTHIA [17] event generator. We include the photon flux and use cuts close to the experimental ones. We first examine the leading-order charm spectra for direct and resolved photons, estimate the cross section in the two cases, and study how the fragmentation process alters the charm spectra in the string model. Then we add flavour excitation and gluon splitting and find that also in this case they give a significant contribution to the charm cross section, especially for resolved photons.

We consider charm photoproduction in an $e^{\pm}$p collision (820 GeV protons and 27.5

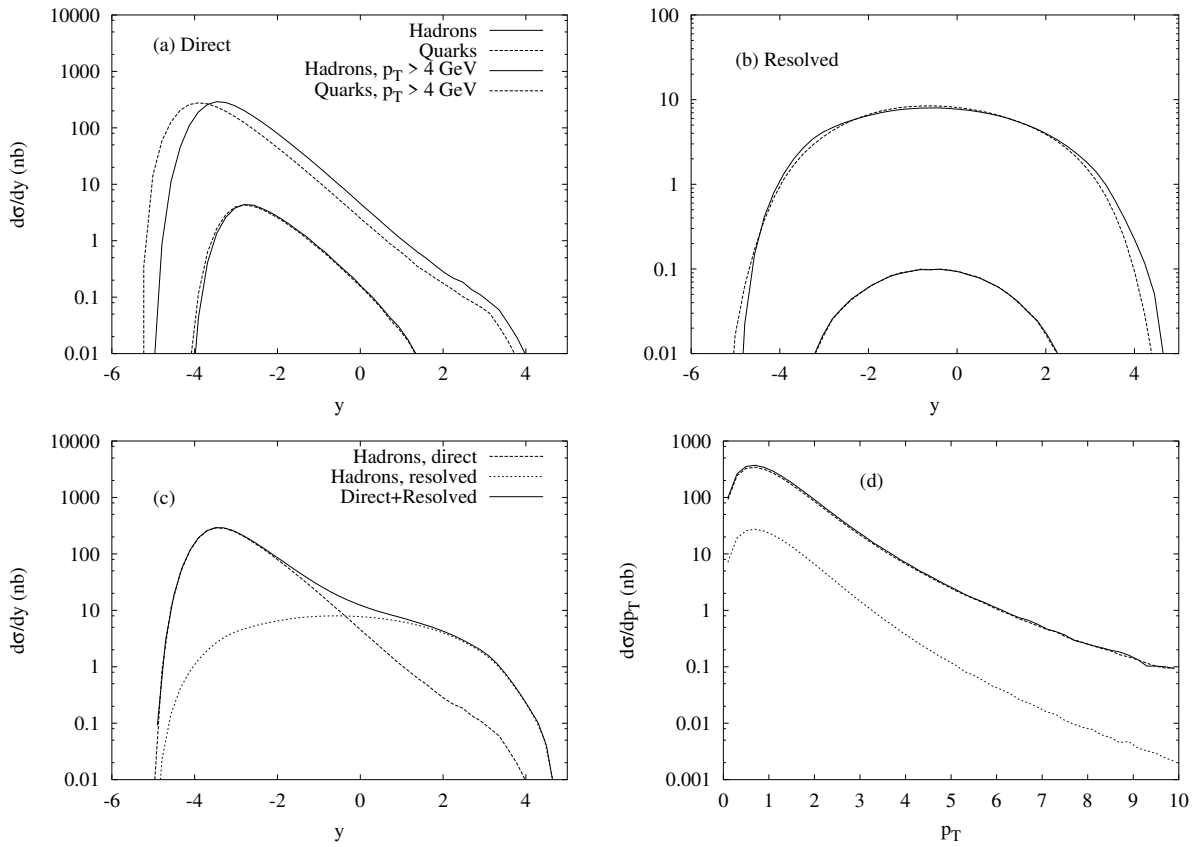

Figure 23: Leading order distribution of charmed hadrons and quarks in rapidity: (a) direct and (b) resolved photons. Comparison of resolved and direct processes in (c) rapidity and (d) transverse momentum.

GeV electrons) with real photons ($Q^2 < 1$ GeV) and rather large energy in the γp CMS system ($130 < W_{\gamma \mathrm{p}} < 280$) using some different $p_\perp$-cuts. The analysis is done in the γp center of mass system using true rapidity ($y = \frac{1}{2}\ln(\frac{E+p_z}{E-p_z})$) as the main kinematical variable. The photon (electron) beam is incident along the negative z-axis.

To leading order, the massive matrix elements producing charm are the fusion processes $\mathrm{g}\gamma \to \mathrm{c\overline{c}}$ (direct), $\mathrm{gg} \to \mathrm{c\overline{c}}$ and $\mathrm{q\overline{q}} \to \mathrm{c\overline{c}}$ (resolved). Fig. 23 shows the distribution of charmed quarks and charmed hadrons separated into these two classes. For direct photons the hadrons are shifted in the direction of the proton beam, since both charm quarks are colour-connected to the proton beam remnant. In a resolved event the photon also has a beam remnant, so the charmed hadron is shifted towards the beam remnant it is connected to. Also in this case the drag effect is a small-$p_\perp$ phenomenon.

The drag effect is illustrated in Fig. 24 where the average rapidity shift in the hadronization, $\langle \Delta y \rangle = \langle y_{\mathrm{Hadron}} - y_{\mathrm{Quark}} \rangle$, is shown as a function of y_{Hadron}. For direct photons and central rapidities the shift is approximately constant. The increasing shift for large rapidities is due to an increased interaction between the proton remnant and the charmed quark when their combined invariant mass is small. At large negative rapidities there is no corresponding effect because there is no beam remnant there. The drop of $\langle \Delta y \rangle$ in this region is a pure edge effect; only those events with below-average Δy can give a very negative y_{Hadron}. For resolved photons the shift is in the direction of the proton and photon beam remnants. Note that what is plotted is only the mean. The width of Δy is generally larger than the mean, so the shift can go both ways. For example the

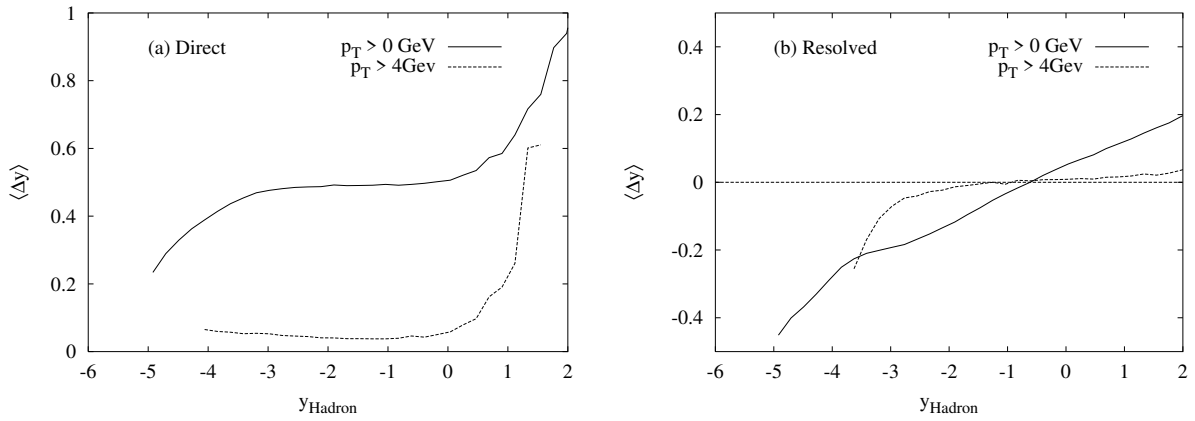

Figure 24: Rapidity shift $\langle \Delta y \rangle = \langle y_{\mathrm{Hadron}} - y_{\mathrm{Quark}} \rangle$ for (a) direct and (b) resolved photons as a function of rapidity.

quarks at very small rapidities ($y \lesssim -5$) in Fig. 23b will almost all be shifted with $\Delta y > 0$ but hadrons produced there will, on the average, come from quarks produced at larger rapidities (i.e. $\Delta y < 0$). Hence the apparent contradiction with Fig. 24b by these edge effects. The differences between these figures and Fig. 13 stem exclusively from differences in the event topology.

At HERA energies, flavour excitation and gluon splitting give large contributions to the cross section. In Fig. 25 the cross section is divided into different production channels for direct and resolved photons. We note that the cross sections are of the same order of magnitude, unlike the results in lowest order, and the major contribution in the resolved case is flavour excitation. The details of course depend on the parameterization of the photon structure.

The double peak structure in the flavour excitation process for direct photons is because the charm quark in the beam remnant at low $p_\perp$ is also included. This peak disappears when a $p_\perp$ cut is introduced (Fig. 25c).

5 Summary and outlook

In this study, we have further developed a model for the production and hadronization of heavy quarks in hadronic collisions. While the emphasis lies on the modelling of the nonperturbative phenomena, the two cannot be fully separated and therefore have to be considered in common. Thus the road we take for the production stage — using a three-component picture of pair creation, flavour excitation and gluon splitting together giving the heavy-flavour cross section — is not very economical if viewed in isolation. A next-to-leading-order matrix elements description could do the job much better, at least at current energies; only at higher energies could the possibility of extensive showering histories make a fixed-order approach inferior to our leading-log showering one. The real difference is instead that our approach also defines the environment in which the heavy quarks are produced: partons from the hard interaction, from its associated showers and from beam remnants, joined in a specific order by colour-confinement strings. And, as we have attempted to show, it is essential to have that background if one wants to understand the production of the heavy hadrons, not only the heavy quarks.

This article represents the third main one on heavy flavours from the Lund group.

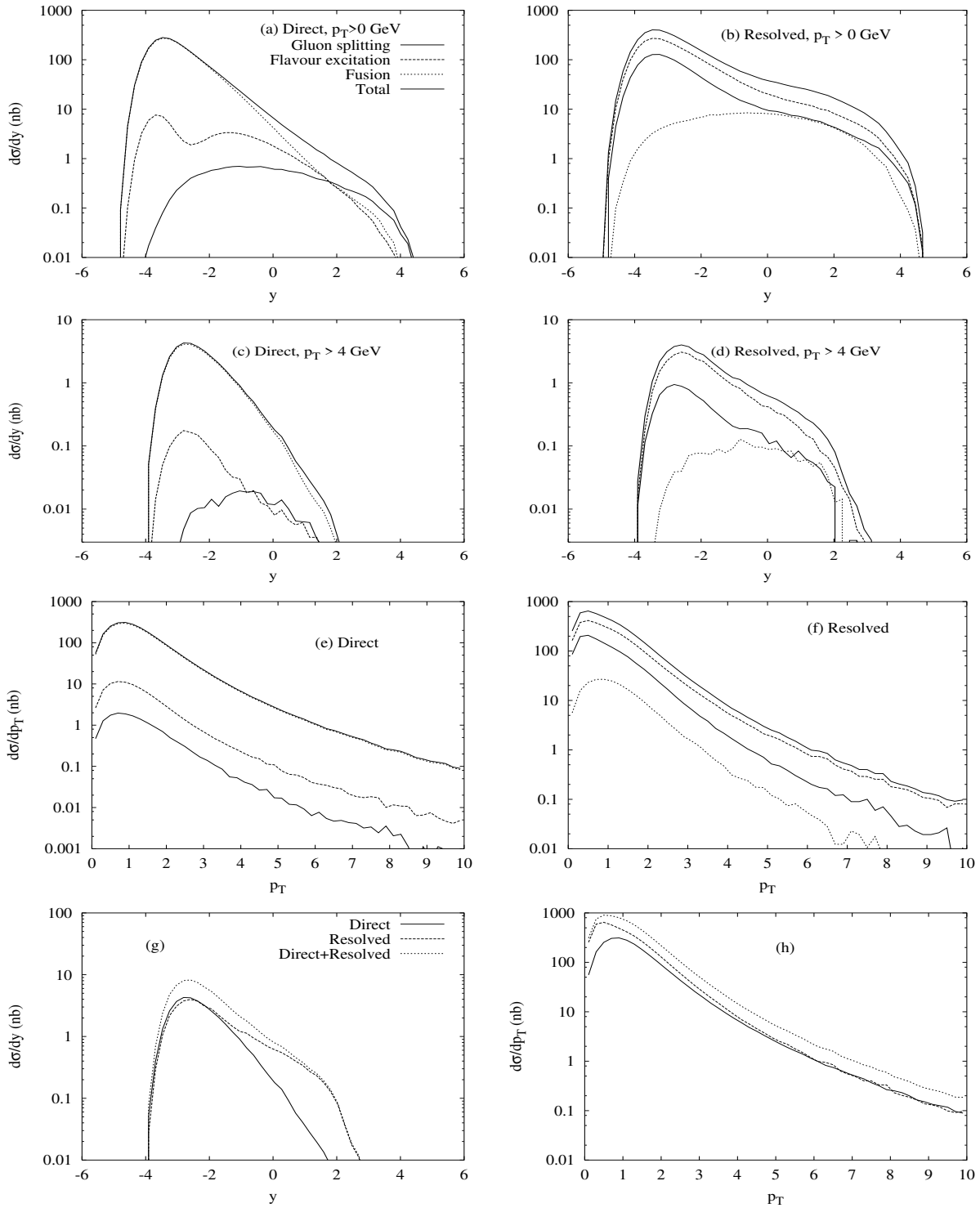

Figure 25: The cross section for charm hadrons divided into different production mechanisms and different photon structure. (a) Direct and (b) resolved photons with $p_\perp > 0$ GeV. (c) Direct and (d) resolved photons with $p_\perp > 4$ GeV. (e) Direct and (f) resolved photons in $p_\perp$. We add the components together for (g) rapidity ($p_\perp > 4$ GeV) and (h) transverse momentum.

The basic ideas were already established almost twenty years ago, so the path taken since has been evolutionary rather than revolutionary. At the time of the first study [9], neither the model nor the data were good enough more than to hint at the validity of the basic principles. In the subsequent years the modelling was gradually improved [17], and fits to some model parameters were performed by at least one experimental collaboration [8]. In our more recent study [10] it was therefore possible to start at a higher level, and introduce a technically somewhat more sophisticated re-implementation of the same basic ideas. This trend is continued in the current article, where some further model details have been improved. The main difference, however, is that we here have considered a wider range of observables, for more different production channels, and for several experimental configurations.

The basic ideas are not particularly controversial today, but the outcome may often be unexpected and counterintuitive. For instance, it is well known, from LEP and other e^+e^- machines, that the heavy hadron only takes a fraction of the heavy-quark energy, i.e. that the pull of the string in the hadronization stage 'slows down' the heavy quark. However, before one has studied the colour topology of heavy-flavour production in hadronic events, and done some trivial Lorentz boost brain gymnastics, it is not equally obvious that exactly the same phenomenon could 'speed up' the heavy quark here. Or: it is not unreasonable that a heavy quark could pick up one of the beam valence flavours to form a hadron, but the extent to which this can happen over a wide range of longitudinal and transverse momenta may come as a surprise.

The studies here have also put the finger on a few other interesting phenomena, such as:

- The extrapolation from charm to bottom quarks.
- The importance of heavy flavour production through flavour excitation and gluon splitting.
- The kinematics of backward evolution in the initial state shower.
- Scale choices in the parton shower.
- The importance of colour flow.
- The matching of cluster decay and string fragmentation of low-mass colour singlets.
- The details of the collapse mechanism.
- The choice and importance of beam remnant distribution functions.
- The choice and importance of intrinsic $k_\perp$ smearing.
- High-$p_\perp$ asymmetries.
- The influence of the photon structure.
- The limitations of the model.

While not as spectacular as the colour drag and flavour asymmetry ones above, they help to put flesh on the bones of our understanding of hadronization. Experimental results on the yet untested features clearly would be welcome.

A topic not discussed in this paper is cosmic ray physics where the momentum spectra of charm and bottom hadrons has implications for the rate of prompt leptons and neutrinos in atmospheric cascades [46]. Also here our improved modelling may affect the traditional flux calculations.

It is important to remember that the predictions can be wrong. Hopefully not in a qualitative fashion, but quite possibly in a quantitative one. For instance, it is all well to assume we can control the colour topologies at fixed-target energies, where there is a very small number of participating partons and thereby of separate string pieces. At

high energies, the more extensive parton showers and especially the increased rate of multiple parton–parton interactions could well mess up our tidy picture of colour flow, and thereby of single-particle spectra and correlations. If so, we would like to believe that heavy flavours here could be used as a probe for such effects.

Of course, our approach is not the only one that has been proposed for the hadronization of heavy quarks [47]. Especially the intrinsic charm model [48] is still very actively pursued. It is not unlikely that several mechanisms may coexist, but we have also encountered no evidence to indicate that the ones outlined by us are not the dominant ones. However, as always, more data may provide new insights also in this regard.

A final reflection is that B physics will remain a major topic of study for many years to come, because of the interest in CP violation studies. Furthermore, many of these studies will require a tagging of both beauty hadrons in an event. One can therefore foresee large data sets that will allow many detailed tests, beyond the ones shown here. It also appears plausible that charm hadron samples can be extracted as a by-product, where, as we have seen, many of the predicted effects are larger. Hopefully we will therefore enjoy a gradually improved level of understanding.

References

[1] B. Andersson, G. Gustafson, G. Ingelman and T. Sjöstrand, Phys. Rep. **97** (1983) 31

[2] C. Peterson, D. Schlatter, I. Schmitt and P. Zerwas, Phys. Rev. **D27** (1983) 105

[3] T. Mannel, Rept. Prog. Phys. **60** (1997) 1113;
and references therein

[4] M. Basile et al., Nuovo Cim. **A66** (1981) 129;
ACCMOR Collaboration, R. Bailey et al., Phys. Lett. **132B** (1983) 237;
NA27 Collaboration, M. Aguilar-Benitez et al., Phys. Lett. **B161** (1985) 400;
NA32 Collaboration, S. Barlag et al., Z. Phys. **C49** (1991) 555

[5] WA82 Collaboration, M. Adamovich et al., Phys. Lett. **B305** (1993) 402

[6] WA92 Collaboration, M. Adamovich et al., Nucl. Phys. **B495** (1997) 3

[7] E769 Collaboration, G.A. Alves et al., Phys. Rev. Lett. **72** (1994) 812

[8] E791 Collaboration, E.M. Aitala et al., Phys. Lett. **B371** (1996) 157

[9] B. Andersson, H.-U. Bengtsson and G. Gustafson, Lund preprint LU TP 83–4 (1983)

[10] E. Norrbin and T. Sjöstrand, Phys. Lett. **B442** (1998) 407

[11] B.L. Combridge, Nucl. Phys. **B151** (1979) 429

[12] P. Nason, S. Dawson and R.K. Ellis, Nucl. Phys. **B327** (1989) 49; erratum ibid. **B335** (1990) 260;
W. Beenakker, R. Meng, G.A. Schuler, J. Smith and W.L. Van Neerven, Nucl. Phys. **B351** (1991) 507

[13] S. Frixione, M.L. Mangano, P. Nason and G. Ridolfi, Nucl. Phys. **B431** (1994) 453

[14] E. Laenen, J. Smith and W.L. van Neerven, Phys. Lett. **B321** (1994) 254;
N. Kidonakis and J. Smith, Phys. Rev. **D51** (1995) 6092;
M. Cacciari, M. Greco and P. Nason, J. High Energy Phys. **05** (1998) 007;
F.I. Olness, R.J. Scalise and W.-K. Tung, Phys. Rev. **D59** (1999) 014506

[15] T. Sjöstrand, Phys. Lett. **157B** (1985) 321

[16] DELPHI Collaboration, P. Abreu et al., Phys. Lett. **B418** (1998) 430

[17] T. Sjöstrand, Comput. Phys. Commun. **82** (1994) 74

[18] G. Marchesini, B.R. Webber, G. Abbiendi, I.G. Knowles, M.H. Seymour and L. Stanco, Comput. Phys. Commun. **67** (1992) 465

[19] M.H. Seymour, Nucl. Phys. **B436** (1995) 163;
D.J. Miller and M.H. Seymour, Phys. Lett. **B435** (1998) 213

[20] M.L. Mangano, CERN-TH/99-337, hep-ph/9911256, to appear in the Proceedings of EPS HEP '99, Tampere, Finland, 15-21 July 1999

[21] L. Lönnblad, Comput. Phys. Commun. **71** (1992) 15

[22] A. De Rújula, H. Georgi and S.L. Glashow, Phys. Rev. **D12** (1975) 147

[23] CTEQ Collaboration, H.L. Lai et al., Eur. Phys J. **C12** (2000) 375

[24] M. Glück, E. Reya and A. Vogt, Z. Phys. **C53** (1992) 651

[25] H.-U. Bengtsson, Comput. Phys. Commun. **31** (1984) 323

[26] E.D. Bloom and F.J. Gilman, Phys. Rev. **D4** (1971) 2901;
J.J. Sakurai, Phys. Lett. **46B** (1973) 207;
H. Fritzsch, Phys. Lett. **67B** (1977) 217;
R.A. Bertlmann, G. Launer and E. de Rafael, Nucl.Phys. **B250** (1985) 61;
and references therein.

[27] E. Braaten, S. Narison and A. Pich, Nucl. Phys. **B373** (1992) 581

[28] Particle Data Group, C. Caso et al., Eur. Phys. J. **C3** (1998) 1

[29] T. Sjöstrand, Nucl. Phys. **B248** (1984) 469

[30] A. Capella and J. Tran Thanh Van, Z. Physik **C10** (1981) 249

[31] EMC Collaboration, M. Arneodo et al., Z. Physik **C36** (1987) 527;
L. Apanasevich et al., Phys.Rev.**D59** (1999) 074007;
G. Miu and T. Sjöstrand, Phys. Lett.**B449** (1999) 313;
C. Bálazs, J. Huston and I. Puljak, hep-ph/0002032

[32] T. Sjöstrand and M. van Zijl, Phys. Rev. **D36** (1987) 2019

[33] G. Gustafson, U. Pettersson and P. Zerwas, Phys. Lett. **B209** (1988) 90;
T. Sjöstrand and V.A. Khoze, Z. Physik **C62** (1994) 281, Phys. Rev. Lett. **72** (1994) 28;
G.Gustafson and J.Häkkinen, Z. Physik **C64** (1994) 659;
L. Lönnblad, Z. Physik **C70** (1996) 107;
Š. Todorova–Nová, DELPHI Internal Note 96-158 PHYS 651;
J. Ellis and K. Geiger, Phys. Rev. **D54** (1996) 1967, Phys. Lett. **B404** (1997) 230;
B.R. Webber, J. Phys. **G24** (1998) 287

[34] A. Edin, G. Ingelman and J. Rathsman, Phys.Rev. **D56** (1997) 7317

[35] M.L. Mangano, P. Nason and G. Ridolfi, Nucl. Phys. **B372** (1992) 295; Nucl. Phys. **B405** (1993) 507

[36] M. Chaichian and A. Fridman, Phys. Lett. **B298** (1993) 218

[37] H1 Collaboration, S. Aid et al., Nucl. Phys. **B472** (1996) 32;
ZEUS Collaboration, J. Breitweg et al., Eur. Phys. J. **C6** (1999) 67; hep-ex/0003018

[38] H1 Collaboration, C. Adloff et al., Nucl. Phys. **B545** (1999) 21;
ZEUS Collaboration, J. Breitweg et al., Eur. Phys. J. **C12** (2000) 35

[39] WA92 Collaboration, M. Adamovich et al., Phys. Lett. **B385** (1996) 487

[40] E791 collaboration, E.M. Aitala et al., Eur. Phys. J. **C4** (1999) 1

[41] D. Barberis, C. Gemme and L. Malferrari, in *Heavy Quarks at fixed target*, eds. H.W.K. Cheung and J.N. Butler p. 179

[42] E. Norrbin, in *Heavy Quarks at fixed target*, eds. H.W.K. Cheung and J.N. Butler p. 228 (hep-ph/9812460)

[43] E687 Collaboration, P.L. Frabetti et al., Phys. Lett. **B370** (1996) 222

[44] P. Nason et al., hep-ph/0003142, to appear in the Report of the "1999 CERN Workshop on SM physics (and more) at the LHC", P. Nason, G. Ridolfi, O. Schneider G.F. Tartarelli, P. Vikas (conveners)

[45] G.A. Schuler and T. Sjöstrand, Nucl. Phys. **B407** (1993) 539; Z. Phys. **C73** (1997) 677

[46] M. Thunman, G. Ingelman and P. Gondolo, Nucl. Phys. Proc. Suppl. **B43** (1995) 274; Astropart. Phys. **5** (1996) 309

[47] V. Barger, F. Halzen and W.Y. Keung, Phys. Rev. **D25** (1982) 112;
P. Mazzanti and S. Wada, Phys. Rev. **D26** (1982) 602;
G.I. Lykasov and M.N Sergeenko, Z. Phys. **C56** (1992) 697;
R.C. Hwa, Phys. Rev. **D51** (1995) 85;
V.A. Bednyakov, Mod. Phys. Lett. **68** (1995) 61;
A.K. Likhoded and S.R. Slabospitsky, hep-ph/9710476;
E. Cuautle, G. Herrera and J. Magnin, Eur. Phys. J. **C2** (1998) 473;
O. Piskounova, Nucl. Phys. **B50** (Proc. Suppl.) (1996) 179;
J. Dias de Deus and F.O. Durães, hep-ph/9803449

[48] S.J. Brodsky, P. Hoyer, C. Peterson and N. Sakai, Phys. Lett. **93B** (1980) 451;
R. Vogt and S.J. Brodsky, Nucl. Phys. **B478** (1996) 311;
G. Ingelman and M. Thunman, Z. Phys. **C73** (1997) 505